PHYSICAL REVIEW B VOLUME 27, NUMBER 6 15 MARCH 1983

Point defects in α-Al_2O_3:Mg studied by electrical conductivity, optical absorption, and ESR

H. A. Wang, C. H. Lee, and F. A. Kröger
Department of Materials Science, University of Southern California, Los Angeles, California 90089-0241

R. T. Cox
Département de Recherche Fondamentale, Section de Résonance Magnétique, Centre d'Etudes Nucléaires de Grenoble, 85X, F-38041, Grenoble Cédex, France
(Received 15 March 1982)

Total and partial ionic and electronic c-axis dc conductivities were measured for single-crystal Al_2O_3:8 ppm Mg as a function of oxygen pressure and temperature. The sample is unsaturated at $T > 1360$ °C but is saturated in equilibrium with a spinel precipitate phase at lower temperatures. The results are analyzed to give ionic mobility, thermodynamic parameters of oxidation reduction of Al_2O_3, and the solubility of MgO as a function of temperature. Oxidized samples are grayish purple due to the presence of a broad absorption band with maximum at 480 nm. Discoloration can occur by reduction (at high temperature) or by precipitation (at $T < 1000$ °C); both proceed from the surface, involving migration of oxygen out of or of Al into the crystal. An explanation for the rapid diffusion regulating precipitation below 1000 °C is proposed. Recoloration at low temperature proceeds without a front and possibly involves oxygen diffusing into the sample along dislocations or subgrain boundaries. Hole-release studies at low temperature indicate that the hole binding energy in the defect Mg_{Al}^{x}, $E_a \leq 0.68$ eV. The combined results of the present work suggest that free holes move as large, rather than small, polarons and that $E_a = 0.68$ eV.

INTRODUCTION

Previous work on single crystals of Al_2O_3 doped with Mg (Ref. 1) has shown that the crystal is colorless after annealing at high temperature in a reducing atmosphere, while it is colored gray-purple after annealing in an oxidizing atmosphere. Electron-spin resonance (ESR) shows that the color is due to the presence of the paramagnetic defect Mg_{Al}^{x}, an Mg^{2+} ion with a trapped hole.[2] The hole is localized on one of the six anions surrounding the cation site occupied by the magnesium impurity. That is, an accurate model of the defect is an O^- ion on an O^{2-} site next to Mg^{2+}. In parallel with the color changes, changes are observed in the high-temperature conductivity, the conductivity being mainly ionic at low p_{O_2} and electronic (by holes) at high p_{O_2}.[3] The holes are created by ionization of the neutral acceptors

$$Mg_{Al}^{x} \rightleftarrows Mg'_{Al} + h^{\cdot} ,$$

with an equilibrium constant K_a^{Mg}. The symbols used here and further on are those proposed by Kröger and Vink.[4,5] Subscripts indicate the site; superscript x, the prime, and the dot indicate effective charges that are zero, negative, and positive, respectively. Vacancies are indicated by V, and interstitial sites by i. The charge of Mg'_{Al} is compensated mainly by $V_O^{\cdot\cdot}$ and $Al_i^{\cdot\cdot\cdot}$ and, if donors D are present, by $D^{\cdot}$, the hole concentration being always smaller than that of Mg'_{Al}. Oxidation reduction and the accompanying color change were found to occur surprisingly fast at temperatures as low as 1000 K, and on this basis the major ionic defect was assumed to be $Al_i^{\cdot\cdot\cdot}$ (Ref. 1). However, the rapidity of the process seems too large to be explained on the basis of ionic mobility determined from the ionic conductivity,[3] and it has been suggested that the rapid change could be due to introduction or removal of hydrogen[6] as observed in other cases.[7,8] Analysis of the electrical data led to values of the c-axis parallel and transverse ionic mobility,[3] and to the position of the Mg'_{Al} level.[3,9] Both results need checking: The absolute value of the ionic mobility was $\sim$10 times smaller than a value found[10] for Al_2O_3:Co; the level position was deduced on the basis of the assumption that the crystal at

$T < 1500$ °C was not in equilibrium with the atmosphere, an assumption that may be incorrect if oxidation reduction occurs with a large rate even at much lower temperatures. Finally, the concentration of Mg in the crystal discussed in Ref. 3 was of the same order as that of other impurities. This paper describes results in a more heavily doped crystal for high-temperature conductivity and for the kinetics of composition and color change. Included are also relevant results of a study of the kinetics of the thermal release of holes trapped by Mg^{2+} ions during ultraviolet irradiation at low temperature.

Electrical measurements and part of the optical experiments were performed at the University of Southern California, Los Angeles; electron-spin resonance and further optical work were carried out at the Centre d'Etudes Nucléaires de Grenoble.

EXPERIMENT

Sample preparation

The single crystal of Al_2O_3:Mg studied in this paper was a 2-cm-diam., 8-cm-long boule grown using the Verneuil oxygen and/or hydrogen-flame fusion process by Y. Grange, Cristaltec Division of Laboratoire d'Electronique et de Technologie de l'Informatique (85X,F-38041, Grenoble Cédex, France). The feed powder was no. 4 Al_2O_3, La Pierre Synthetique-Baikowski (Avenue des Romains, Annecy, France), 99.99% pure, doped with 200 ppm Mg by weight.

As grown, the boule had a purple coloration showing the presence of uncompensated Mg_{Al}^{x} centers, presumably created as the boule cooled down in air after the flame had been cut off (the flame itself is reducing). The boule was then "stabilized" by heating at 1800 °C for 10 h under a low-oxygen pressure: argon in contact with graphite heating elements. This procedure relieves strain, reducing the tendency of the Verneuil-grown crystals to crack during cutting, a particularly troublesome problem with Mg-doped Al_2O_3 crystals. After this treatment, the boule was colorless. It was then recolored by heating in air at 1600 °C for one day. The resultant state will be referred to as the "as-received state."

In the as-received state the boule had a grayish-purple coloration (some observers have described it as pink-violet) which was reasonably uniform throughout its volume. The purple color is proof of the absence of a high concentration of iron impurity. In earlier trials at Cristaltec laboratory, Al_2O_3:Mg boules grown from less pure feed material had often turned out yellow or brown. Colors of this kind have also been reported in the literature,[11,12] including the crystal studied in Ref. 3. We also found that deliberate double doping with Mg plus Fe gives very strong yellow or brown colors, resulting from the low-energy tail of absorption shoulders in the violet and ultraviolet regions. ESR spectroscopy of such samples shows a strong ESR spectrum unambiguously attributable to Fe^{5+} (a $3d^3$ ion[13]); this leads us to believe that the absorption shoulders correspond to ligand-metal charge transfer transitions of Fe^{4+} and/or Fe^{5+} ions present as a result of charge compensation of Mg^{2+}. (The normal charge state of iron in alumina, Fe^{3+}, has no strong optical absorptions in the visible range.)

Four 0.5-g samples, cut from four different points in the boule, were analyzed for Mg and Fe at the analytical division of the Centre d'Etudes Nucléaires de Grenoble, and at the Centre de Recherche Ugine-Kuhlmann, F-38560 Jarrie, France. The samples were powdered in sapphire mortars and analyzed spectrographically by comparison with standard doped alumina samples (detection limits in parts per million by weight: 2 for Mg and 5 for Fe). The results were $[Mg]/[Al_2O_3]=13$, 14, 29, and 34 ppm for the four samples, and $[Fe]/[Al_2O_3]$ detectable but not exceeding 10 ppm for the three samples. The Mg analyses are believed to have absolute accuracy $\pm 20\%$.

The analyses show that the Mg is inhomogeneously distributed in the boule. The average value of the Mg concentration is 22 ± 10 ppm $= (2.16 \pm 1) \times 10^{18}$ cm^{-3}, but as we shall see, there are indications that the samples on which our experiments were done were in the low-concentration range with an effective Mg concentration of only 8×10^{17} cm^{-3}. Both values are much smaller than the 200 ppm Mg added to the feed powder used for crystal growth. Large losses often occur for volatile dopants in Verneuil growth, but a comparative chemical analysis of an unstabilized Al_2O_3:Mg sample suggests that reduction in Mg content by a factor of only 4 may have occurred during the 1800 °C stabilization treatment—this point needs further investigation. Comparison of the Mg and Fe analyses indicates that the atomic ratio [Mg]/[Fe] in our boule is between $\frac{5}{1}$ and $\frac{2}{1}$.

Electrical measurements were performed on cylindrical samples of 12 mm diam. and 1–2 mm thickness with the c axis perpendicular to the plane. Pieces of $\simeq 8 \times 3.3 \times 3.3$ mm^3 with the c axis perpendicular to the 8×3.3 face were used in the optical and spin resonance measurements.

The studies of the hole-release process at $T \lesssim 300$ K were performed with crystals grown from Al_2O_3 powders doped with 200 ppm Mg plus 200 ppm Fe and with 200 ppm Mg plus 200 ppm Cr, respectively. Analyses were not done for these crystals. As mentioned earlier, the Mg + Fe crystal had a brown color. The Mg + Cr crystal was colored orange, a color associated with the presence[14] of Cr^{4+}. ESR observations at 4 K (Ref. 13) have confirmed that the Cr^{4+} ESR signal[14] (undetectable at room temperature) is present for orange rubies counterdoped with Mg.

Measurement techniques

dc electrical conductivity was measured by a two-probe method, a volume guard being used to eliminate surface and gas-phase conduction. Ionic transference numbers t_i were determined from the emf

$$E=(RT/nF)\int_{\mathrm{I}}^{\mathrm{II}} t_i \ln p_{O_2}$$

of concentration cells of the type

$$\mathrm{Pt},(p_{O_2})_{\mathrm{I}}/Al_2O_3/\mathrm{Pt},(p_{O_2})_{\mathrm{II}},$$

again measured using the volume guard. F is the Faraday charge and n the number of charges involved with migration of two oxygen ions (or $\frac{4}{3}$ aluminum ions); $(p_{O_2})_{\mathrm{I}}$ and $(p_{O_2})_{\mathrm{II}}$ indicate oxygen pressures at the Pt contacts at the sides I and II of the sample. Well-defined oxygen pressures were established with the aid of oxygen, air, technical nitrogen (monitored with a zirconia gauge), and CO/CO_2 mixtures. For a detailed description of the apparatus and experimental procedure, see Ref. 10.

Conductivities were measured allowing either long times after a change of conditions in order to achieve equilibrium or allowing only little time (nonequilibrium or partial equilibrium). Optical absorption was determined at room temperature in the wavelength range 300–2000 nm with double-beam spectrophotometers. The spectrum was obtained either by comparing intensities of transmitted light for a beam passing through the sample and a reference beam passing through a colorless Al_2O_3:Mg sample of identical thickness or by subtracting calculated reflection losses from the absorption measured for the colored sample.

For a study of the kinetics of the color change at temperatures less than 1000 °C, crystals were annealed for various times in oxidizing or reducing atmospheres. In cases where a color front was observed, the rate of penetration of the boundary between colored and discolored regions was used to determine a chemical diffusion constant, similar to the method used for studying diffusion in Al_2O_3:Ti.[15] ESR measurements of the concentrations of Mg_{Al}^{x} centers at room temperature were made with Varian E-line spectrometers operating at 9 GHz. At this frequency, the six lines in the 35-GHz spectrum[2] of the Mg_{Al}^{x} center corresponding to the six symmetry-related orientations of the Mg^{2+}–trapped-hole axis are not resolved; the spectrum appears as a single line about 30 G wide, whose amplitude, shape, and position varies slightly with magnetic field orientation ($g=2.011$ and 2.019 for $\vec{H}\|c$ and $\vec{H}\perp c$, respectively).

For relative concentration measurements (accurate to $\pm 10\%$ or better in comparisons of different samples or of different heat-treated states of the same sample) the amplitude of this ESR line was compared to that for an oxidized Al_2O_3:Mg reference sample; this was done at a fixed orientation of the field with respect to the c axis, chosen near 80° to avoid interference with iron and chromium impurity lines. Absolute concentrations, believed to be accurate to $\pm 25\%$, were obtained by comparison of the double integral of the Mg_{Al}^{x} line of the reference sample with the double integrals of the ESR lines of (a) a ruby ESR standard from the National Bureau of Standards[16] (NBS) and (b) a Varian pitch-in-KCl standard. These two comparisons gave results differing not more than 10%; the ruby standard was preferred.

Direct comparison to the NBS ruby standard with double integration was also made to determine the Mg_{Al}^{x} concentration in an optical sample which was used in measurements of the oscillator strength of the 480-nm band of Mg_{Al}^{x}.

In ESR studies of the ultraviolet-induced creation and the subsequent thermal annealing of metastable Mg_{Al}^{x} centers at −70 to 25 °C, samples of dimensions a few cubic millimeters were placed in cooling gas in a glass tube which traversed the ESR cavity. They were irradiated with (10–100)-mW, (334–364)-nm light from an argon laser through an optical window in the cavity wall.

RESULTS

Electrical measurements

Figure 1 shows conductivity isotherms at 1450, 1500, and 1600 °C and partial conductivities $\sigma_i = t_i\sigma$

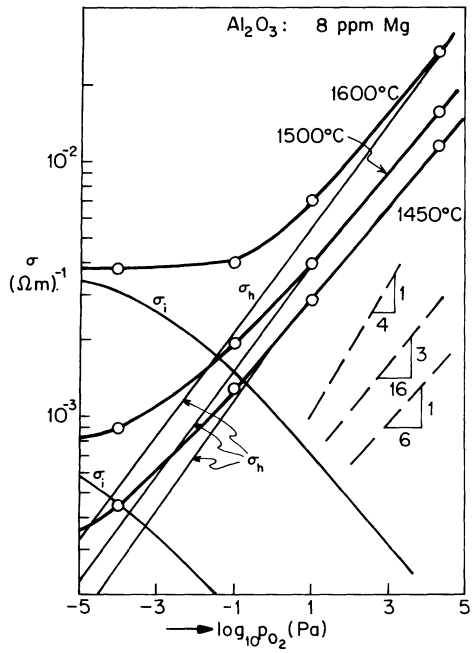

FIG. 1. Conductivity as $f(p_{O_2})$ at 1450, 1500, and 1600 °C and partial conductivities $\sigma_i = t_i\sigma$ and $\sigma_{el} = \sigma_h = (1-t_i)\sigma$ using t_i values of Fig. 2.

and $\sigma_{el} \equiv \sigma_h = (1-t_i)\sigma$, using t_i values from Fig. 2. Figure 2 shows the corresponding emf measurements for a cell

$$\mathrm{Pt},(p_{O_2})_{\mathrm{I}}/\mathrm{Al_2O_3}/\mathrm{Pt},(p_{O_2})_{\mathrm{II}}$$

and the ionic transference numbers deduced from it by differentiation for $(p_{O_2})_{\mathrm{II}}$:

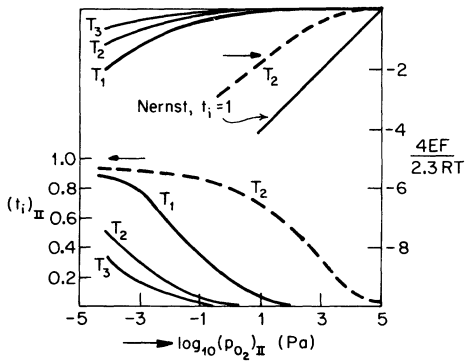

FIG. 2. Reduced emf $4EF/2.3RT$ of an oxygen concentration cell with $(p_{O_2})_{\mathrm{I}} = 10^5$ Pa, $(p_{O_2})_{\mathrm{II}}$ variable, at $T_1 = 1600$, $T_2 = 1500$, and $T_3 = 1450$ °C, and the corresponding values of $(t_i)_{\mathrm{II}}$. A dashed line gives modified values for 1500 °C to fit the data of Fig. 5.

$$(t_i)_{\mathrm{II}} = \frac{2.3RT}{4F}\left[\frac{\partial E}{\partial \log_{10}(p_{O_2})_{\mathrm{II}}}\right]_{(p_{O_2})_{\mathrm{I}}}.$$

Figure 3 gives conductivities at various oxygen pressures as $f(1/T)$. Inspection of Figs. 1–3 shows that the conductivity at $p_{O_2} \geq 10^{-1}$ Pa is largely electronic; that at $p_{O_2} = 10^{-4}$ Pa is of mixed character. The bend in curve 5 of Fig. 3 results from the variation in the ratio σ_i/σ_h with temperature. Curves 1*a* and 1*b* refer to the crystal as received, but kept at temperature for times long enough to achieve equilibrium with the atmosphere. The points of curve 1*b* at $T < 1300$ °C were obtained after an anneal of 12 h, the points at 1400 °C after 2 h. Measurements at $T < 1300$ °C after a shorter anneal gave points on curves parallel to curve 1*b* but a factor of 2–3 above it. This was believed to be due to inhomogeneous precipitation in the as-received material resulting from inhomogeneity in the Mg content, which was removed by longer annealing. Similar shifts were observed in the ESR measurements (Fig. 8). Curve 2 was obtained after the sample had been annealed at 1600 °C for 0.5 h. Points were taken with decreasing temperature with waiting times of $\simeq 0.5$ h each. Curves 1*a*, 2*a*, and 2*b* are represented by

$$\sigma_h = 710\exp[(1-1.6\ \mathrm{eV})/kT]\ , \tag{1}$$

curve 1*b* by

$$\sigma_h = 1.34\times 10^5 \exp[(-2.4\ \mathrm{eV})/kT]\ , \tag{2}$$

and curve 7 by

$$\sigma_h = 31.6\exp[(-1.66\ \mathrm{eV})/kT]\ , \tag{3}$$

all in units of $\Omega^{-1}\mathrm{m}^{-1}$. Conductivities at $p_{O_2} \geq 10$ Pa are largely electronic (by holes); ionic contributions become appreciable at $p_{O_2} \leq 10$ Pa.

Optical and ESR measurements at room temperature

Neutral acceptors Mg_{Al}^{x} stable at room temperature were studied by optical and ESR methods on samples cooled at a rate fast enough to freeze in diffusion processes that could destroy Mg_{Al}^{x}.

Optical studies

Figure 4 shows the optical spectra of samples annealed for 24 h at 1500 °C under various oxygen

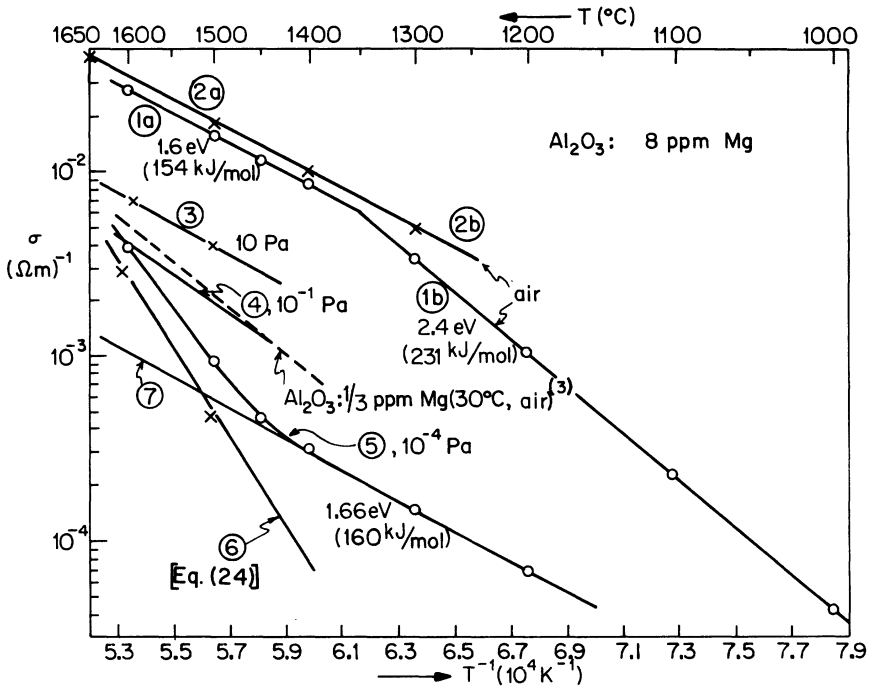

FIG. 3. Temperature dependence of dc conductivity $||c$ at $p_{O_2}=2\times10^4$ Pa (air) (curves 1*a*, 1*b* and 2*a*, 2*b*), 10^2 and 10^{-1} Pa (curves 3,4), and 10^{-4} Pa (curve 5). Curves 6 and 7 represent σ_i and $\sigma_h=\sigma-\sigma_i$.

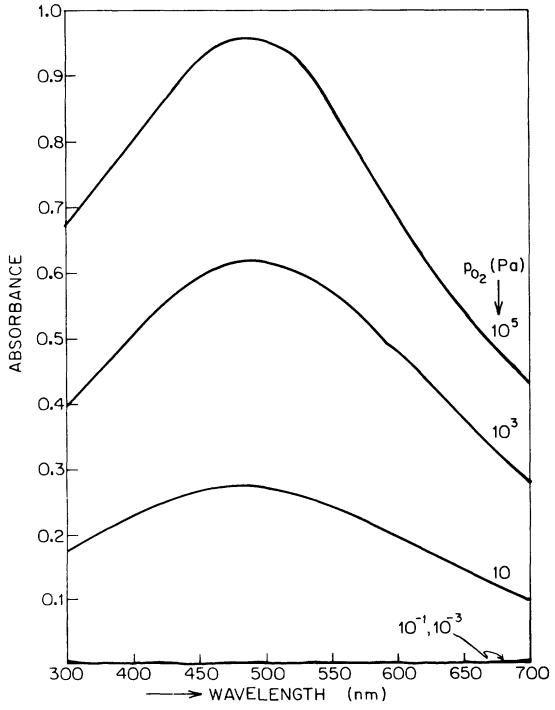

FIG. 4. Optical absorption for light propagating $||c$ for crystals annealed for 24 h at 1500°C under different oxygen pressures.

pressures, quenched by removal from the furnace. For the higher p_{O_2} values, a broad band peaking at about 480 nm is observed. The tail of this band (not shown) extends to about 1200 nm in the infrared region: No absorption is detected between 1200 and 2000 nm.

Given the changes in color with the efforts made to improve crystal purity, we believe that the 480-nm absorption band seen in Fig. 4 represents the optical absorption of the Mg_{Al}^{x} center better than the spectra published previously. An additional peak at 350 nm found in the crystal investigated in Ref. 3 and assigned there also to Mg_{Al}^{x} must have been due to an impurity, probably iron. It is the improved transparency in the violet region (<480 nm) that gives the grayish-purple tint (combined of red and violet) as distinct from yellow-brown colors.

Nevertheless, the 480-nm band of Fig. 4 is still not symmetric when plotted against energy, suggesting that other bands lie under its high-energy side. These may represent residual impurities or, alternatively, the Mg_{Al}^{x} absorption itself may have a complex substructure. The low-energy side of the band up to the 480-nm peak is close to Gaussian shaped, and we have arbitrarily determined the oscillator strength f for this peak by assuming it to be

symmetric. That is, we integrated from 2000 nm to the band peak and doubled the result (the full width at half height of the Gaussian band defined in this way is 1.3 eV). For light polarized perpendicular to c (an unpolarized beam propagating parallel to c) we obtain for this symmetric part of the band

$$f_{\perp}=0.07\pm0.02 \tag{4}$$

with f defined by

$$Nf=8.21\times10^{16}[n/(n^2+2)^2]\int\alpha(E)dE\ .$$

Here N is the Mg^x_{Al} concentration per cm^3, which was determined by ESR, n is the refractive index, α is the adsorption coefficient equal to $\ln_{10}$ $\times$ [(absorbance)/(thickness)] in cm^{-1}, and E is the optical energy in eV; this is Dexter's corrected version of the Smakula formula, Eq. (6) of Ref. 17.

As a guide to future use of optical spectroscopy for determining the Mg^x_{Al} concentration, we note that we found (in cm^2):

$$\frac{\alpha_{\perp,480}}{\mathrm{cm}^{-1}}\Big/\frac{N}{\mathrm{cm}^{-3}}=8.8\times10^{-18}\ . \tag{5}$$

From measurements in light propagating perpendicular to c, we found that $f_{\parallel}/f_{\perp}\simeq1.8$. The peak position appears identical in the two polarizations.

The quite high oscillator strength and the large bandwidth of the optical absorption are similar to those observed for other trapped-hole centers in oxides, e.g., for V'_{Mg} and Li^x_{Mg} in MgO (Refs. 18 and 19) and Al^x_{Si} (the "smoky quartz" center) in SiO_2.[20] A plausible explanation of such absorptions is that they correspond to charge transfer transitions (also called "polaron" transitions) in which the hole is transferred between two of the anion sites neighboring the cation defect that traps it.[21] Such a transition is expected to be polarized along the anion-anion direction; the polarization ratio found for Mg^x_{Al} corresponds to a transition moment oriented at 37° to the c axis, which is close to the orientations (33°) of 6 of the 12 edges of the O_6 octahedron containing a cation site in the sapphire structure. Figure 5 shows the absorption coefficient at 480 nm as a function of $\log_{10}p_{O_2}$ together with some absolute Mg^x_{Al} concentrations measured by ESR for samples quenched after anneals at 1500° and 1600 °C in atmospheres with different p_{O_2}.

Annealing an as-received oxidized crystal in air or argon at temperatures ranging from 640 to 900 °C caused discoloration to move in from the surface with a rate increasing with increasing temperature. The penetration depth at constant temperature was $\propto t^{1/2}$, indicating limitation by diffusion with a constant diffusion coefficient. The effect is the same for both atmospheres during the anneal. It should be noted, however, that the concentration of residual centers, too small to be detected by optical absorption, but detectable by ESR, may be different in the two cases. Such differences do not, however, affect the rate of diffusion of the color front, which is described by a chemical diffusion coefficient

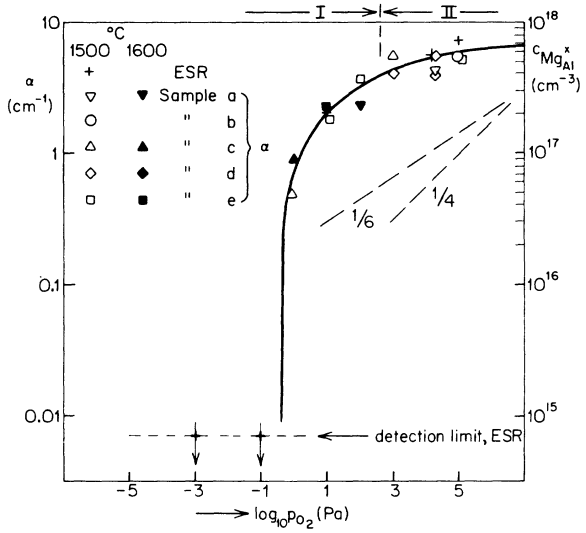

FIG. 5. Concentration of Mg^x_{Al} centers determined by ESR (pluses) and optical absorption at 480 nm for light propagating $||c$ (other symbols) for crystals annealed for 24 h at 1500 and 1600 °C under various oxygen pressures. I and II refer to the similarly marked oxygen pressure ranges in Fig. 14.

$$\tilde{D}=2.5\times10^{-6}\exp[(-0.8\ \mathrm{eV})/kT]\ , \tag{6}$$

in units of m^2s^{-1}. As seen in Fig. 6, it has absolute values which at 1400 °C are $\simeq10^4$ times larger than those for Al_2O_3:Ti (Ref. 15) (which is limited by electron migration[22,23]) and 10^9 and 10^{12} times larger than the reported values of the self-diffusion constants of Al (Ref. 24) and O (Refs. 25 and 26). The activation energy is smaller than that of either of these. $\tilde{D}$ is, however, of the same order (and has a similar activation energy) as the chemical diffusion coefficient determined from the variation by reduction of the conductivity of polycrystalline Al_2O_3:Mg (Lucalox, grain size $d=30\mu$m) between 1100 and 1350 °C.[27]

For anneals in air, samples several millimeters thick appeared colorless after complete penetration of the color front when the annealing temperature was below about 900 °C but, as seen in the next sec-

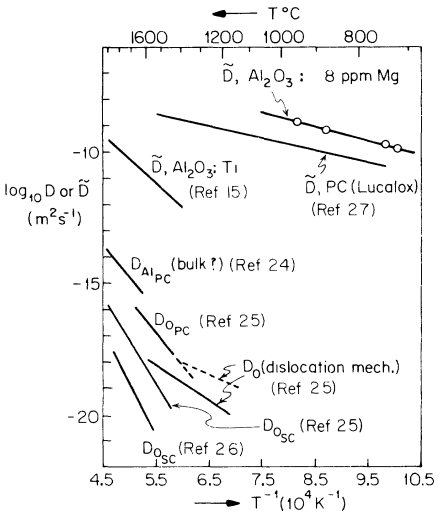

FIG. 6. Chemical diffusion coefficients $\tilde{D}$ for discoloration of Al_2O_3:Mg^x_{Al} single crystal at $T<1000$ °C and of Al_2O_3:Ti^x_{Al} by oxidation at $T>1400$ °C (Ref. 15), conductivity change of polycrystalline Al_2O_3 (Lucalox) at $1320>T>1100$ °C (Ref. 27), and self-diffusion coefficients for Al (Ref. 24) and O (Refs. 25 and 26); sc is single crystal, pc is polycrystal.

tion, small concentrations of Mg^x_{Al} centers could still be detected by the ESR technique down to at least 800 °C. Above 900 °C, discoloration is partial: Residual color is visible with intensity increasing with the annealing temperature. Samples discolored at $T<900$ °C are rapidly recolored, to an intensity increasing with temperature, on heating in air at higher temperatures. Contrary to what was observed for the discoloration at $T<900$ °C, this recoloration occurred homogeneously: No color front moved in from the surface. Figure 7 shows the absorption coefficient at 480 nm and the corresponding concentration of Mg^x_{Al} centers as a function of the time of annealing in air at 950 °C for a sample initially colored at 1500 °C in air, then discolored by a 64-h anneal at 800 °C in air: Recoloration is complete in $\simeq$200 min. This is $\simeq$10 times slower than would be expected on the basis of Eq. (6) should the recoloration involve movement of a front (which it does not). The absence of coloration at $t<60$ min and the sudden increase for $t\geq 70$ min is no doubt due to the same effect responsible for the cutoff seen in Fig. 5; an addition of oxygen below a certain critical amount not producing coloration. Annealing in N_2+10 Pa O_2 at 1050 °C of samples discolored at $T<900$ °C also leads to recoloration. However, annealing in CO/CO_2 mixtures with $p_{O_2}\simeq 10^{-4}$ Pa does not produce recoloration. Thus the oxidizing power of the atmosphere is an important factor in recoloration, the latter occurring only when p_{O_2} is larger than a critical value which appears to correspond to the cutoff observed in Fig. 5. This cutoff was found to be independent of temperature at high temperatures where the sample is unsaturated, but is expected to shift to higher p_{O_2} at lower temperatures where the concentration of MgO dissolved in the Al_2O_3 phase is diminished as a result of precipitation.

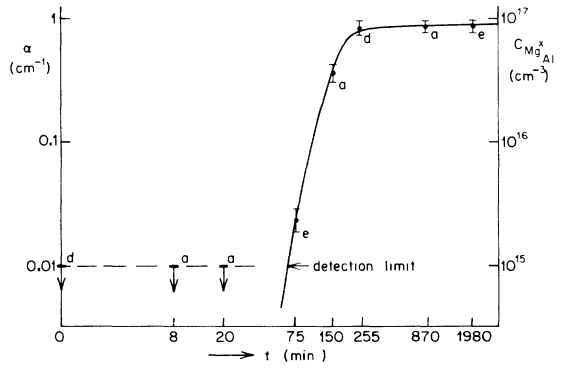

FIG. 7. Absorption coefficient (α) at 480 nm and the corresponding concentration of Mg^x_{Al} centers for samples *a*, *d*, and *e* annealed for various times at 950 °C in air after an initial coloration treatment in air at 1500 °C and a discoloration anneal at 800 °C in air (64 h).

The intensity of color established by an oxidizing anneal appeared to be independent of whether the sample was previously annealed at a higher or at a lower temperature. Similar results were obtained in an ESR study to be reported on in the next section.

The effect of p_{O_2} indicates that recoloration involves oxidation by in-diffusion of oxygen or outdiffusion of aluminum. Since no front is observed, the diffusion may be a two-step process: relatively rapid penetration along dislocations or subgrain boundaries followed by a slow penetration from these into the subgrains, the latter process determining the time needed to complete the recoloration process.

Discoloration upon annealing in air at $T<900$ °C as observed for a sample preannealed at 1600 °C in air did not occur with samples preannealed for a long time in air at $T>1650$ °C. This suggests that the discoloration at low temperatures is not just a reduction process, but that it involves precipitation of the dissolved MgO as a second phase—the long anneal at high T destroying nuclei of the new phase, therewith preventing the formation of precipitates.

ESR measurements

In order to see how $[Mg^x_{Al}]$ varies with the temperature of annealing, samples of $3.3\times 3.3\times 8$ mm^3

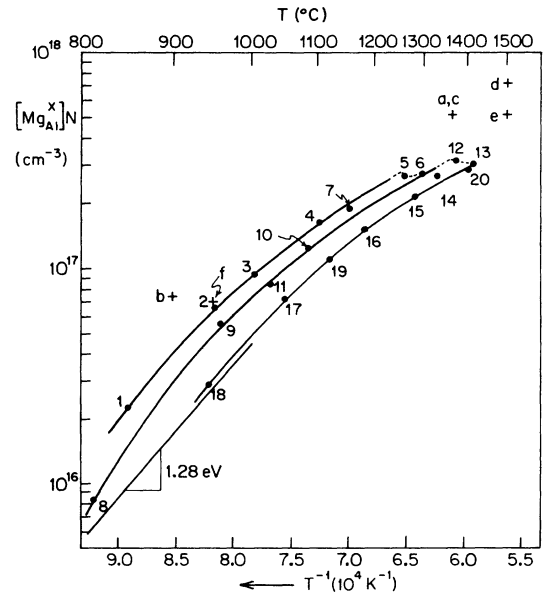

FIG. 8. Concentrations of Mg_{Al}^{x} centers as a function of temperature of annealing in air determined by electron-spin resonance in samples cooled to room temperature: points determined in sequence of numbering; *a*, *b*, and *c* as described in the text, *d* colored at 1500 °C at $p_{O_2}=10^5$ Pa, *e* colored at 1500 °C at $p_{O_2}=2\times10^4$ Pa (air), *f* sample *d* annealed in air.

were heated in air in an alumina-tube furnace for various times at temperatures in the range 800—1450 °C. After each heating period, they were pushed out of the tube (time taken about 3 s) and allowed to cool in air. From the time of disappearance of their red glow, we estimate that the samples cooled from, e.g., 1400 °C to below 900 °C in less than 30 s. Quenching from the higher temperatures sometimes introduced cracks in the sample. This does not interfere with ESR measurements; optical measurements then become impossible, however, and diffusion along cracks can alter the kinetics.

After each quenching, the Mg_{Al}^{x} concentration was measured by ESR at room temperature. Results are plotted in Fig. 8. Optical spectra were not taken in this series of experiments but the visual intensity of the purple color followed closely the changes in Mg_{Al}^{x} concentrations measured by ESR.

In Fig. 8 points 1—20 represent the average of the quenched-in Mg_{Al}^{x} concentrations for two samples 4 and 6 that were taken together through a long series of anneals. These samples showed remarkably parallel behavior: Although their equilibration rates were sometimes different, the final concentration for sample 6 was always 85%±10% of that of sample 4.

Although no systematic study of the kinetics was made in the series 1,...,20, the samples were annealed for successive periods at some of the temperature points to ensure that a well-defined state had been reached. The major part of the increase or decrease in concentration induced by increasing or decreasing the annealing temperature occurred very rapidly, even at quite low temperatures. For discoloration this rapid change corresponds to the penetration of the discoloration front as described in the preceding section. It was more than 90% complete in a time of order 10 h at $T\simeq800$ °C, of order 10 min at $T\simeq1400$ °C. For points 1—20 of Fig. 8, the annealing time was long enough to complete this rapid change to within a few percent accuracy, often 10—100 times longer than necessary. On bleaching at temperatures <1000 °C the ESR signal strength usually overshot the final value, falling initially to a low value but rising quickly back to a final plateau.

Following the initial rapid change at the higher temperatures (>1100 °C) there was a slow loss of Mg_{Al}^{x} centers, proceeding at an erratic rate. On the other hand, at the lower temperatures, after the above-mentioned overshoot and rise back to a pla-

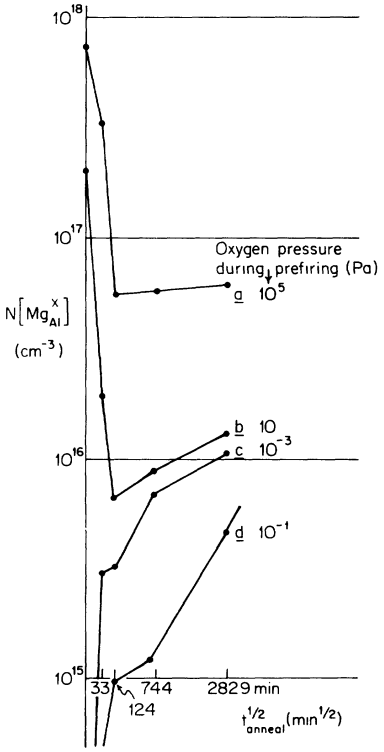

FIG. 9. Concentrations of Mg_{Al}^{x} as a function of the time of reanneal at 950 °C in air for samples prefired at 1500 °C at various oxygen pressures.

teau value, the concentration crept slowly upwards at about 1−3 % per day. These two types of slow change were still continuing at the end of each annealing sequence; the data of Fig. 8 represent mainly the state of partial equilibrium achieved on completion of the rapid first-stage changes. Kinetics curves showing the overshoot effect in another series of measurements are given in Fig. 9.

As shown in Fig. 8, the main result of this series is that the quenched-in Mg_{Al}^{x} concentration is a regularly increasing function of temperature. Except for a complication discussed below, the concentration produced by a given anneal was independent of whether the previous anneal was done at higher or lower temperature: The coloration and/or discoloration process appears to be reversible.

The slow second-stage loss of centers at the highest temperatures complicates matters slightly because it appears to be irreversible. Thus, following the high-temperature anneals at points 5 and 6 and later at points 12, and 13 of Fig. 8, subsequent anneals define a new concentration versus temperature curve lying below previous points as clearly seen in the figure. After point 13, annealing times were minimized and the upward-going points 19 and 20 lie on the downward-going curve 13−18, indicating that the rapid coloration and/or discoloration process is reversible.

Points *a*, *b*, and *c* in Fig. 8, representing three anneals in air of another sample (no. 8, initially in the as-received condition), also illustrate reversibility: The two short anneals at 1360 °C (points *a* and *c*) give almost identical Mg_{Al}^{x} concentrations despite the intervening discoloration experiment at 900 °C (point *b*). Anneals at higher T in air (point *e*), or oxygen (point *d*) for two other samples give similar values.

With sample 8 it was verified that successive (short) anneals at 1360 °C always gave the same Mg_{Al}^{x} concentration to high precision, despite small variations in the speed of removing the sample from the furnace. This and the apparent reversibility mentioned above suggest that the quenching is fast enough to freeze in at least the fraction of the high-temperature defect structure that is of interest in ESR, namely acceptors plus thermally ionized acceptors with their corresponding holes which yield neutral acceptors after cooling.

Point *b* for sample 8 is the final value of the ESR signal after 15 increasingly long air anneals at 900 °C after preoxidation at 1360 °C. The sample remained uncracked throughout. The Mg_{Al}^{x} concentration decreased approximately linearly with $t^{1/2}$ until it began to flatten out to its equilibrium value.

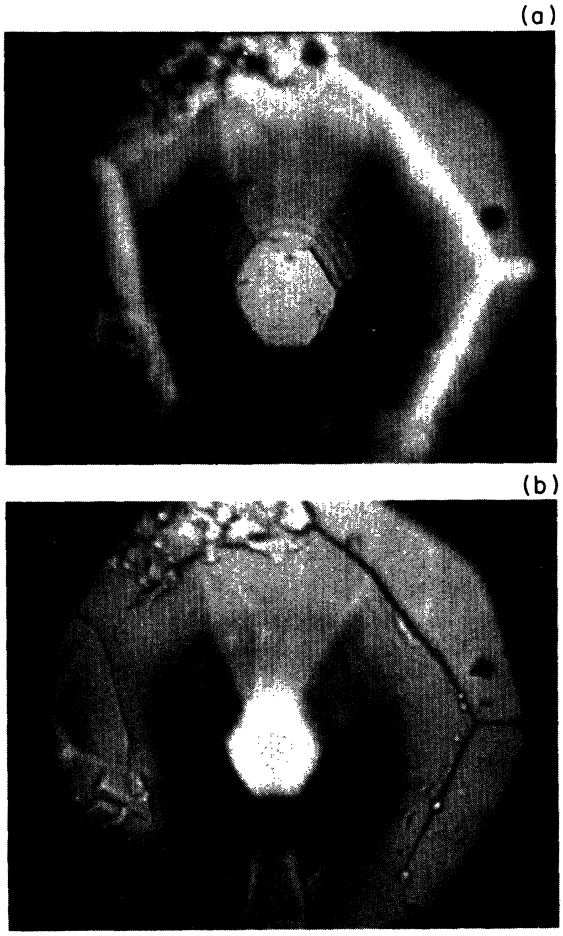

FIG. 10. Microscope picture (magnification 400×) of the surface of a crystal discolored by a prolonged anneal at 900 °C etched for 10 min with borax at 800 °C.

FIG. 11. TEM picture (magnification 8500×) showing the presence of precipitates along dislocation lines.

This is as expected from the $t^{1/2}$ dependence of the rate of migration of the discoloration front observed in the absorption studies described earlier. The loss of centers measured by ESR agreed with that deduced from rough measurements of the position of the color front observed in this sample.

Microstructure

Etching of polished surfaces with hot phosphoric acid gave etch pits indicating a dislocation density of 10^9-10^{10} m^{-2}. Subgrain boundaries were not observed.

In samples discolored by annealing at 900°C, etching for 10 min with borax gave rise to hexagonally shaped etch pits: Fig. 10(a) gives the picture focused on the bottom of the pit; Fig. 10(b) gives the corresponding one focused at the rim of the pit. Investigation of the pit area with the energy dispersive x-ray analyzer in the secondary-emission monitor shows only Al. Similar pits were not found in

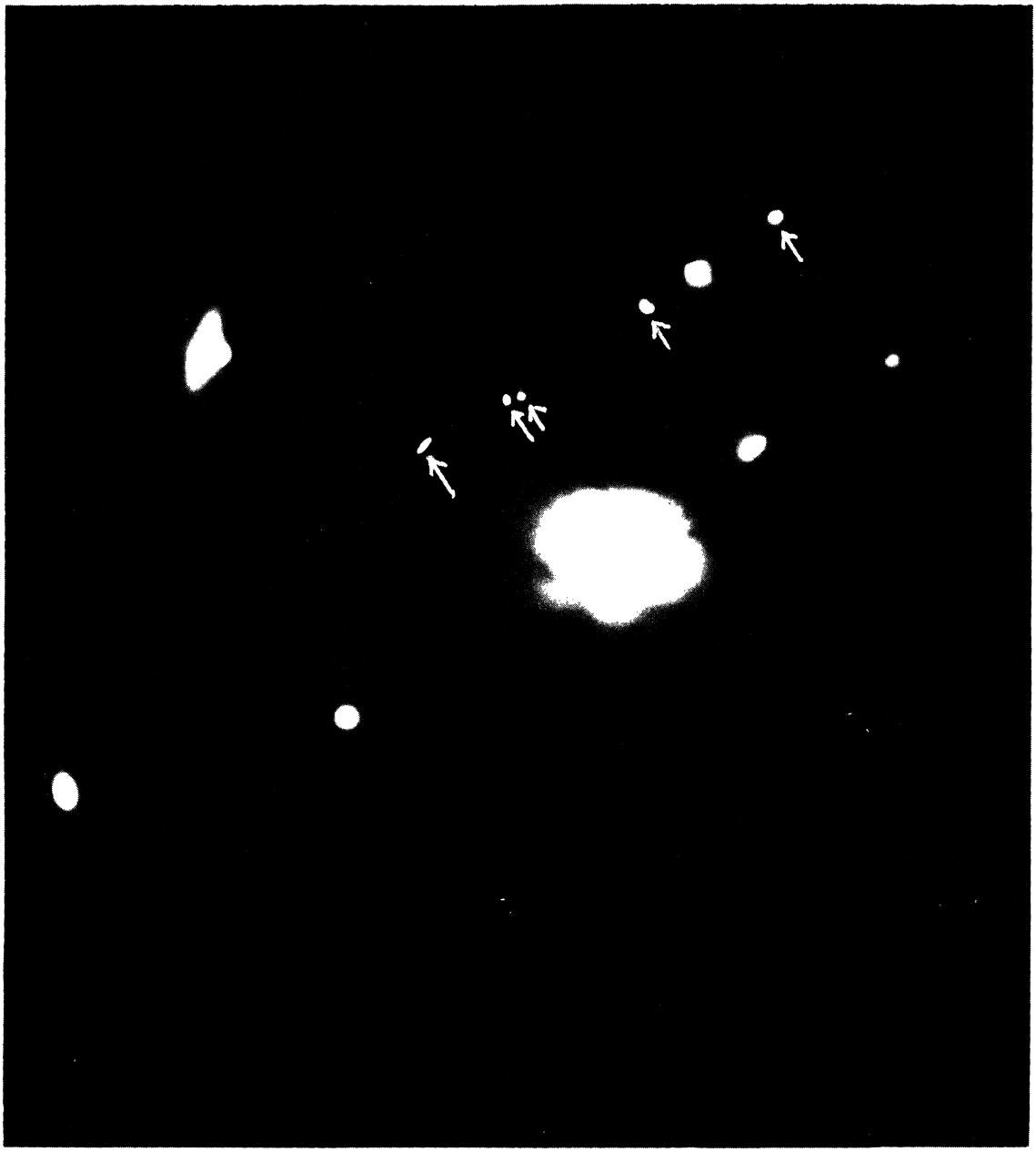

FIG. 12. Electron diffraction pattern of a precipitate and its surroundings show the spots due to Al_2O_3 and extra spots caused by the precipitate (the latter marked by arrows).

crystals annealed for a long time at 1450–1600 °C at $p_{O_2}=10^{-4}$ Pa. This suggests that the pits were formed by preferential etching away of precipitates. The hexagonal shape is characteristic of the Al_2O_3 rather than of the precipitates (spinel) which are cubic and have at most trigonal symmetry [perpendicular to the (111) plane].

Figure 11 shows a transmission electron-microscope picture of a sample discolored at 900 °C after thinning by grinding and argon-ion bombardment. The figure shows the presence of precipitates at dislocations. Electron diffraction of the precipitate area shows diffraction spots of the precipitate in addition to the spots of Al_2O_3 (Fig. 12). The pattern was not analyzed, but the precipitate phase should be a spinel, $MgAl_2O_4$ (Refs. 28 and 29) or $Mg_{0.8}Al_2O_{3.8}$ (Ref. 30).

Low-temperature hole-release studies in Al_2O_3:Mg+Fe or Al_2O_3:Mg+Cr

Included here are some relevant results from an ESR study of the physics of photoionization and annealing processes at $T<300$ K in Al_2O_3 crystals double doped with Mg and a transition metal. This study yields the binding energy for a hole trapped by Mg^{2+}, i.e., the acceptor ionization energy.

These experiments were done with a brown (Mg + Fe)-doped sample and an orange (Mg + Cr)-doped sample. Before the experiments, ESR spectroscopy showed (i) a strong Mg_{Al}^{x} signal with no detectable Fe^{3+} for the Mg + Fe sample and (ii) no Mg_{Al}^{x} signal with a strong Cr^{3+} signal for the Mg + Cr sample. As discussed in the sample preparation section (see also Ref. 31 and references therein), Fe and Cr appear to act as donors with respect to Mg, with the Fe_{Al}^{x} and Cr_{Al}^{x} level above the Mg'_{Al} level, i.e., Fe^{4+} and Cr^{4+} can compensate the charge of Mg^{2+}. Then the results indicate that Mg is undercompensated in the Mg + Fe sample ([Mg] > [Fe]), overcompensated in the Mg + Cr sample ([Mg] < [Cr]).

Irradiation with (334–364)-nm light at low temperature (i) tripled the Mg_{Al}^{x} signal and created an Fe^{3+} signal for the Mg + Fe sample and (ii) created a Mg_{Al}^{x} signal and increased the Cr^{3+} signal for the Mg + Cr crystal. Although other impurities and lattice defects might participate in the electronic processes, we consider that the dominant effect is

$$Mg'_{Al}+D^{\cdot}\rightarrow Mg_{Al}^{x}+D^{x}\,, \tag{7}$$

where D = Fe or Cr.

The exact excitation mechanism is uncertain.

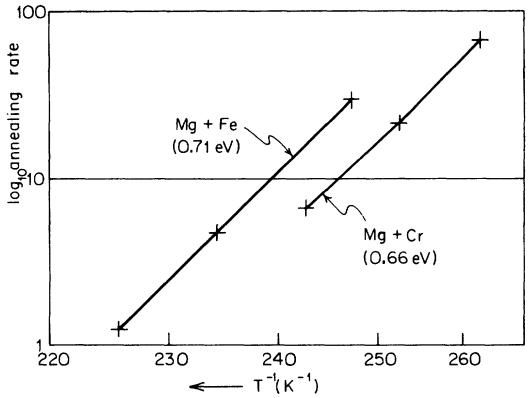

FIG. 13. Rate of hole release as $f(T)$ from Mg_{Al}^{x} formed at low temperature by uv irradiation of Mg + Cr and Mg + Fe doped samples. The release rates have no simple definition since the decay is complex (see text); for both samples the vertical scale units were chosen arbitrarily to correspond to 1000 divided by the time in seconds for 90% annealing.

Two obvious models are (a) photoexcitation of an electron from the valence band to the empty donor level, leaving a hole which migrates to the acceptor or (b) a direct acceptor → donor optical transition.

When the excitation was discontinued, the ESR signals returned to their original levels at a temperature-dependent rate. Decay curves for $[Mg_{Al}^{x}]$ were recorded between −53 and −13 °C (equal to 220–260 K). Annealing was much slower in the Mg + Cr sample than in the Mg + Fe sample at the same temperature. The decay curve at a given temperature did not obey any simple law and, in fact, had quite a different shape for the Mg + Cr and Mg + Fe samples. However, for a given sample, decay curves (covering two decades of concentration change) obtained at different temperatures differed only by a time-scaling factor (expansion or contraction along the time axis). Figure 13 shows that the logarithm of this factor is a linear function of $1/T$ with slope 0.71 and 0.66 eV for the Mg + Fe and Mg + Cr samples, respectively.

The results are nearly the same for the two samples compensated in quite different ways. Moreover, we expect the Fe_{Al}^{x} and Cr_{Al}^{x} levels to lie in the lower half of the band gap. Therefore, we attribute the activation energy found here to hole release rather than to electron release. That is, we consider the annealing to result from thermal release of the hole trapped at Mg_{Al} followed by annihilation of the resulting free hole with an electron at Fe_{Al}^{x} or Cr_{Al}^{x}. It is assumed here that, should the free hole behave as a small polaron with high site-to-site barrier energy (see later), it can migrate fast enough by

phonon-assisted tunneling not to be rate limiting in these low-temperature experiments; the polaron mobility at $kT \sim 0.02$ eV, well below the Al_2O_3 phonon energies of $\sim 0.04-0.1$ eV, would be very much higher than expected from the downward extrapolation of the high-temperature classical jumping mobility.

The average activation energy of hole release for the two samples, $E = 0.68$ eV, can be equal or larger than the thermal energy of ionization of the acceptor Mg_{Al}^{x} with the formation of free holes: larger if there is an activation barrier, equal if there is not. Therefore, the thermal separation of the Mg'_{Al} level from the valence band $E_a = (E_{Mg'_{Al}} - E_v)_{\text{thermal}} \leq 0.68$ eV.

Discussion

Conductivity results at $T \geq 1360$°C represent equilibrium between an unsaturated solid solution Al_2O_3:Mg (with all the Mg present homogeneously dissolved) and the atmosphere. The activation energy of $\simeq 1.6$ eV found for the conductivity in air is somewhat smaller than that of 2–2.4 eV reported in Ref. 3 (see Fig. 3). Contrary to the assumption made there, it must include the effects of oxidation reduction due to the interaction with the atmosphere. The same must apply to curve 2*b*. The different slope of curve 1*b* can be due either to the fact that equilibrium with the atmosphere is not maintained or that part of the Mg has precipitated with formation of a spinel phase.[30] The conditions of the experiments (relatively short waiting times for 2*b*, long waiting times for 1*b*) as well as the results of the microstructure investigations (Figs. 10–12) favor the latter explanation. Since 1*b* is measured starting with the crystal as received and 2*b* after a high-temperature anneal, the difference between the two curves can be attributed to the presence of precipitation nuclei in the crystal as received and the removal of such nuclei by the high-temperature anneal. If this interpretation is correct, the kink point in curve 1 at 1360°C indicates a solubility of MgO in Al_2O_3 in air equal to the Mg content of the crystal. We shall return to this point later.

The isotherms of Fig. 1 combined with the transference numbers of Fig. 2 indicate that $\sigma \simeq \sigma_h$ over most of the p_{O_2} range covered, with σ_h increasing $\propto p_{O_2}^{n}$ with n varying from 1/5.5 to 1/4.7, σ_i becoming important only at low p_{O_2}, and more so the higher the temperature.

Additional information is obtained from the results of optical and ESR experiments shown in Fig. 5 which indicate that $[Mg_{Al}^{x}]_{25°C}$ increases with increasing p_{O_2}, tending towards saturation at a value

TABLE I. Defect reactions and the corresponding mass-action relations, with concentrations in mole fractions.

$3Mg'_{Al} + Al_i^{\cdots} + \frac{3}{4}O_2 \rightleftharpoons 3Mg_{Al}^{x} + Al_{Al}^{x} + \frac{3}{2}O_O^{x}$	$K_{ox,i}^{Mg} = \frac{[Mg_{Al}^{x}]^3}{[Mg'_{Al}]^3[Al_i^{\cdots}]} p_{O_2}^{-3/2}$	(a)
$2Mg'_{Al} + V_O^{\cdot\cdot} + \frac{1}{2}O_2 \rightleftharpoons 2Mg_{Al}^{x} + O_O^{x}$	$K_{ox,V}^{Mg} = \frac{[Mg_{Al}^{x}]^2}{[Mg'_{Al}]^2[V_O^{\cdot\cdot}]} p_{O_2}^{-1/2}$	(b)
$Al_i^{\cdots} + \frac{3}{4}O_2 \rightleftharpoons Al_{Al}^{x} + \frac{3}{2}O_O^{x} + 3h^{\cdot}$	$K_3 = \frac{[h^{\cdot}]^3}{[Al_i^{\cdots}]} p_{O_2}^{-3/4} = K_{ox,i}^{Mg}(K_a^{Mg})^3$	(c)
$V_O^{\cdot\cdot} + \frac{1}{2}O_2 \rightleftharpoons O_O^{x} + 2h^{\cdot}$	$K_4 = \frac{[h^{\cdot}]^2}{[V_O^{\cdot\cdot}]} p_{O_2}^{-1/2} = K_{ox,V}^{Mg}(K_a^{Mg})^2$	(d)
$Mg_{Al}^{x} \rightleftharpoons Mg'_{Al} + h^{\cdot}$	$K_a^{Mg} = \frac{[h^{\cdot}][Mg'_{Al}]}{[Mg_{Al}^{x}]}$	(e)
$3MgO + Al_{Al}^{x} \rightleftharpoons 3Mg'_{Al} + 3O_O^{x} + Al_i^{\cdots}$	$K_{sol,i}^{Mg} = \frac{[Mg'_{Al}]^3[Al_i^{\cdots}]}{a_{MgO}^3}$	(f)
$2MgO \rightleftharpoons 2Mg'_{Al} + V_O^{\cdot\cdot} + 2O_O^{x}$	$K_{sol,V}^{Mg} = \frac{[Mg'_{Al}]^2[V_O^{\cdot\cdot}]}{a_{MgO}^2}$	(g)
$MgO + \frac{1}{4}O_2 \rightleftharpoons Mg_{Al}^{x} + \frac{3}{2}O_O^{x}$	$K_{sol,x}^{Mg} = \frac{[Mg_{Al}^{x}]}{a_{MgO}p_{O_2}^{1/4}} = (K_{sol,V}^{Mg}K_4)^{1/2}/K_a^{Mg}$	(h)
$MgO + Al_2O_3 \rightleftharpoons MgAl_2O_4$	$K_{MgAl_2O_4} = \frac{a_{MgAl_2O_4}}{a_{MgO}a_{Al_2O_3}}$	(i)
$O \rightleftharpoons 2V_{Al}^{'''} + 3V_O^{\cdot\cdot}$	$K_S = [V_{Al}^{'''}]^2[V_O^{\cdot\cdot}]^3$	(j)
$Al_{Al}^{x} + V_i^{x} \rightleftharpoons Al_i^{\cdots} + V_{Al}^{'''}$	$K_{F,Al} = [Al_i^{\cdots}][V_{Al}^{'''}]$	(k)

of $\sim 8\times 10^{17}$ cm^{-3}. This value is smaller than what was believed to be the average Mg content of the crystal, 2.2×10^{18} cm^{-3}. There can be two reasons for this difference: Either the actual Mg content of the crystal is smaller because of errors in the analysis or because of evaporation during the heat treatment, or $\sim 1.4\times 10^{18}$ cm^{-3} donors D are present, compensating part of the Mg_{Al} acceptors, leaving 8×10^{17} cm^{-3} uncompensated. The concentration of Mg_{Al}^{x} at room temperature is the sum of the concentration of Mg_{Al}^{x} and $h^{\cdot}$ at the annealing temperature T, the holes transforming Mg'_{Al} to Mg_{Al}^{x} by trapping during cooling:

$$[Mg_{Al}^{x}]_{25\,^{\circ}C}=[Mg_{Al}^{x}]_T+[h^{\cdot}]_T \ . \tag{8}$$

A priori it is not certain which of these two is the major one. Comparison of the experimental results with theoretical predictions for the shape of isotherms predicted for various models makes it possible to decide both this question and whether or not compensating donors are present. Since self-diffusion of Al (Ref. 24) has been found to be much faster than that of O (Refs. 25 and 26), σ_i must be due to a defect species transporting Al. In the presence of the Mg acceptors these species should be $Al_i^{\cdot\cdot\cdot}$. The observed decrease of σ_i with increasing p_{O_2} must be due to the decrease of $[Al_i^{\cdot\cdot\cdot}]$ as a result of oxidation.

Defect structure models

Defect reactions describing oxidation-reduction processes, ionization of centers, dissolution of $MgAl_2O_4$ in Al_2O_3, and the corresponding mass action relations are given in Table I. Isotherms for defect concentrations as a function of p_{O_2} can be constructed with the aid of these relations complemented by the appropriate neutrality condition and balance equations.

Eight different models have to be considered, dependent on whether the neutrality condition at low p_{O_2} is governed by

$$[Mg'_{Al}]\approx 3[Al_i^{\cdot\cdot\cdot}] \ , \tag{9}$$

$$[Mg'_{Al}]\approx 3[Al_i^{\cdot\cdot\cdot}]+[D^{\cdot}] \ , \tag{10}$$

$$[Mg'_{Al}]\approx 2[V_O^{\cdot\cdot}] \ , \tag{11}$$

or

$$[Mg'_{Al}]\approx 2[V_O^{\cdot\cdot}]+[D^{\cdot}] \ , \tag{12}$$

and on whether

$$[Mg_{Al}^{x}]_{25\,^{\circ}C}\approx[Mg_{Al}^{x}]_T \tag{13}$$

or

$$[Mg_{Al}^{x}]_{25\,^{\circ}C}\approx[h^{\cdot}]_T \ . \tag{14}$$

Exponents n in the expressions for defect concentrations $\propto p_{O_2}^{n}$ for the various models are given in Table II. All isotherms have a region I of low p_{O_2} and a region II at high p_{O_2}. Those for models A and C have a third region (III) at the highest p_{O_2}. Inspection of the results shows that the requirement $\sigma_h\propto[h^{\cdot}]\propto p_{O_2}^{n}$ with $\frac{1}{4}\le n<\frac{1}{6}$ (Fig. 1) rules out models B, D, E, F, G, and H, i.e., $[D]\approx 0$ and $[Mg_{Al}^{x}]_{25\,^{\circ}C}\approx[Mg_{Al}^{x}]_T$. Only models A and C are left, region II in both giving $[Mg_{Al}^{x}]_{25\,^{\circ}C}=[Mg_{Al}^{x}]_T$ independent of oxygen pressure at high p_{O_2} as observed (Fig. 5). Region III is not reached. Since $[D]=0$, $[Mg_{Al}^{x}]_{25\,^{\circ}C}\simeq[Mg_{Al}^{x}]_T\approx[Mg]_{total}\approx 8\times 10^{17}$ cm^{-3}—close to the lower limit of the chemical concentration determination.

According to Table I, relation (e),

$$\frac{[Mg_{Al}^{x}]}{[h^{\cdot}]}=[Mg'_{Al}]/K_a^{Mg} \ .$$

The expression for K_a^{Mg} differs, dependent on whether a band model (large-polaron model) or a small-polaron model applies. In the former case, with a single valence-band maximum at wave-vector zero,[32]

$$K_a^{Mg}=\frac{g'g^{\cdot}}{g^{x}}\left[\frac{2\pi m_h^{*}kT}{h^2}\right]^{3/2}\exp(-E_a/kT) \ . \tag{15}$$

Here E_a is the thermal energy of dissociation of the acceptor $E_a=(E_{Mg'_{Al}}-E_v)_{thermal}$; m_h^{*} is the effective mass of the holes, and the g's are the statistical weights of the species Mg'_{Al}, $h^{\cdot}$, and Mg_{Al}^{x}, equal to 1, 2, and 12, respectively. For small polarons

$$K_a^{Mg}=\frac{g'g^{\cdot}}{g^{x}}N_O\exp(-E_a/kT) \ , \tag{16}$$

with N_O the concentration of the O^{2-} ions, over which the holes would hop, 7.02×10^{22} cm^{-3}. By taking $E_a\le 0.68$ eV as observed, independent of temperature (i.e., neglecting changes in the vibrational entropy), and $m_h^{*}\approx m$, the mass of the electron, Eqs. (15) and (16) give $(K_a^{Mg})_{1500\,^{\circ}C}\approx 3.5\times 10^{17}$ and 1.4×10^{20} cm^{-3}, respectively. With $[Mg'_{Al}]\simeq 8\times 10^{17}$ we find $[Mg_{Al}^{x}]/[h^{\cdot}]\le 2.4$ for the band model (or a larger value for $m_h^{*}<m$) and $\le 6\times 10^{-3}$ for the small-polaron model, the larger

TABLE II. Values of exponents n in $[j] \propto p_{O_2}^{n}$; values for majority defects are underlined; I, II, and III are ranges of oxygen pressure in which the defect structure is dominated by different approximations of the neutrality condition and the Mg balance.

	Model A: $[Mg_{Al}^{x}]$ 25°C$\approx[Mg_{Al}^{x}]_T$			Model B: $[Mg_{Al}^{x}]$ 25°C$\approx[h^{\cdot}]_T$	
	I	II	III	I	II
	$[Mg'_{Al}]\approx 2[V_O^{\cdot\cdot}]$	$[Mg'_{Al}]\approx 2[V_O^{\cdot\cdot}]$	$[Mg_{Al}]\approx[h^{\cdot}]$	$[Mg'_{Al}]\approx 2[V_O^{\cdot\cdot}]$	$[Mg'_{Al}]\approx[h^{\cdot}]$
Mg_{Al}^{x}	$\frac{1}{4}$	$\underline{0}$	$\underline{0}$	$\frac{1}{4}$	0
Mg'_{Al}	$\underline{0}$	$-\frac{1}{6}$	$\underline{0}$	$\underline{0}$	$\underline{0}$
$V_O^{\cdot\cdot}$	$\underline{0}$	$-\frac{1}{6}$	$-\frac{1}{2}$	$\underline{0}$	$-\frac{1}{2}$
$Al_i^{\cdot\cdot\cdot}$	0	$-\frac{1}{4}$	$-\frac{3}{4}$	0	$-\frac{3}{4}$
$h^{\cdot}$	$\frac{1}{4}$	$\frac{1}{6}$	$\underline{0}$	$\frac{1}{4}$	$\underline{0}$

	Model C: $[Mg_{Al}^{x}]$ 25°C$\approx[Mg_{Al}^{x}]_T$			Model D: $[Mg_{Al}^{x}]$ 25°C$\approx[h^{\cdot}]$	
	I	II	III	I	II
	$[Mg'_{Al}]\approx 3[Al_i^{\cdot\cdot\cdot}]$	$[Mg'_{Al}]\approx 3[Al_i^{\cdot\cdot\cdot}]$	$[Mg'_{Al}]\approx[h^{\cdot}]$	$[Mg'_{Al}]\approx 3[Al_i^{\cdot\cdot\cdot}]$	$[Mg'_{Al}]\approx[h^{\cdot}]$
Mg_{Al}^{x}	$\frac{1}{4}$	$\underline{0}$	$\underline{0}$	$\frac{1}{4}$	0
Mg'_{Al}	$\underline{0}$	$-\frac{3}{16}$	$\underline{0}$	$\underline{0}$	$\underline{0}$
$V_O^{\cdot\cdot}$	0	$-\frac{1}{8}$	$-\frac{1}{2}$	0	$-\frac{1}{2}$
$Al_i^{\cdot\cdot\cdot}$	$\underline{0}$	$-\frac{3}{16}$	$-\frac{3}{4}$	$\underline{0}$	$-\frac{3}{4}$
$h^{\cdot}$	$\frac{1}{4}$	$\frac{3}{16}$	$\underline{0}$	$\frac{1}{4}$	$\underline{0}$

	Model E: $[Mg_{Al}^{x}]$ 25°C$\approx[Mg_{Al}^{x}]_T$		Model F: $[Mg_{Al}^{x}]$ 25°C$\approx[h^{\cdot}]_T$	
	I	II	I	II
	$[Mg'_{Al}]\approx 2[V_O^{\cdot\cdot}]+[D^{\cdot}]$	$[Mg'_{Al}]\approx[D^{\cdot}]$	$[Mg'_{Al}]\approx 2[V_O^{\cdot\cdot}]+[D^{\cdot}]$	$[Mg'_{Al}]\approx[h^{\cdot}]+[D^{\cdot}]$
Mg_{Al}^{x}	$\frac{1}{4}$	$\underline{0}$	$\frac{1}{4}$	0
Mg'_{Al}	$\underline{0}$	$\underline{0}$	$\underline{0}$	$\underline{0}$
$V_O^{\cdot\cdot}$	$\underline{0}$	$-\frac{1}{2}$	$\underline{0}$	$-\frac{1}{2}$
$Al_i^{\cdot\cdot\cdot}$	0	$-\frac{3}{4}$	0	$-\frac{3}{4}$
$h^{\cdot}$	$\frac{1}{4}$	0	$\frac{1}{4}$	$\underline{0}$
$D^{\cdot}$	$\underline{0}$	$\underline{0}$	$\underline{0}$	$\underline{0}$

	Model G: $[Mg_{Al}^{x}]$ 25°C$\approx[Mg_{Al}^{x}]_T$		Model H: $[Mg_{Al}^{x}]$ 25°C$\approx[h^{\cdot}]$	
	I	II	I	II
	$[Mg'_{Al}]\approx 3[Al_i^{\cdot\cdot\cdot}]+[D^{\cdot}]$	$[Mg'_{Al}]\approx[D^{\cdot}]$	$[Mg'_{Al}]\approx 3[Al_i^{\cdot\cdot\cdot}]+[D^{\cdot}]$	$[Mg'_{Al}]\approx[D^{\cdot}]+[h^{\cdot}]$
Mg_{Al}^{x}	$\frac{1}{4}$	$\underline{0}$	$\frac{1}{4}$	0
Mg'_{Al}	$\underline{0}$	$\underline{0}$	$\underline{0}$	$\underline{0}$
$V_O^{\cdot\cdot}$		$-\frac{1}{2}$	0	$-\frac{1}{2}$
$Al_i^{\cdot\cdot\cdot}$	$\underline{0}$	$-\frac{3}{4}$	$\underline{0}$	$-\frac{3}{4}$
$h^{\cdot}$	$\frac{1}{4}$	0	$\frac{1}{4}$	$\underline{0}$
$D^{\cdot}$	$\underline{0}$	$\underline{0}$	$\underline{0}$	$\underline{0}$

values corresponding to $E_a = 0.68$ eV. On this basis our previous conclusion that $[Mg_{Al}^{x}]_T > [h^{\cdot}]_T$ thus is inconsistent with the small-polaron model but is in agreement with the large-polaron model for $E_a = 0.68$ eV. Calculations by Colbourn and Mackrodt also indicate that large polarons are more stable

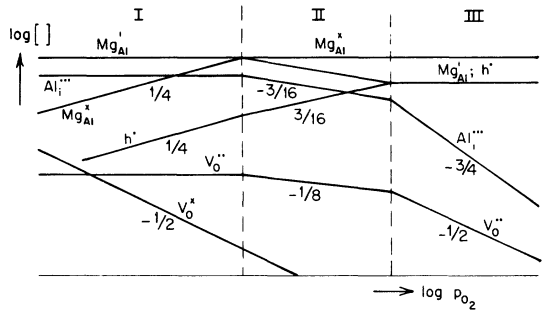

FIG. 14. Isotherms as $f(p_{O_2})$ for Al_2O_3:Mg (model *C*).

than small polarons.[33]

Isotherms for models *C* and *A* (involving interstitial cations and anion vacancies, respectively) are shown in Figs. 14 and 15. According to these isotherms σ_h in region II should increase $\propto p_{O_2}^n$ with $n=\frac{1}{6}$ for model *A*, and $\frac{3}{16}=1/5.3$ for model *C*; in region I both models give $n=\frac{1}{4}$. The partial hole conductivities of Fig. 1 have a constant $n\simeq 1/4.8$ at 1600 °C and show n varying from 1/5.5 at high p_{O_2} to 1/4.7 at low p_{O_2} at 1450 and 1500 °C, demonstrating the expected difference between the values of the exponents in ranges II and I. However, the data are not sufficiently accurate to allow us to decide between the two models.

For both models $[Mg^x_{Al}]_{25\,°C}$ should be independent of annealing temperature for 1500–1600 °C anneals, as actually observed (Figs. 5 and 8). A model different from *A* and *C* with

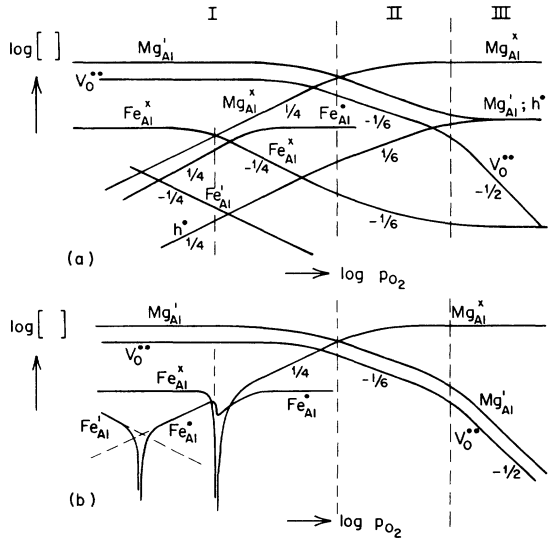

FIG. 15. Defect isotherms as $f(p_{O_2})$ for Al_2O_3:Mg+Fe with [Mg] > [Fe] according to model *A*: (a) high-temperature equilibrium, (b) situation after cooling to room temperature.

$$[Mg'_{Al}]\simeq 2[Mg_i^{\cdot}]\simeq\tfrac{2}{3}[Mg]_{total} \quad (17)$$

proposed by Catlow *et al.*[34] leads to native defect concentrations that are independent of Mg concentration. Since the present sample has a conductivity that is $\sim 7\times$ larger than that of a crystal with a lower Mg content,[3] this model cannot be correct. Equally unacceptable are models dominated by

$$[Mg'_{Al}]=[(Mg_{Al}Mg_i)^{\cdot}]=\tfrac{1}{3}[Mg]_{total} \quad (18)$$

or

$$[Mg'_{Al}]=[(Mg_{Al}Mg_i)^{\cdot}]\,,$$

with

$$[(Mg_{Al}Mg_iMg_{Al})^x]=\tfrac{1}{3}[Mg]_{total}\,, \quad (19)$$

which lead to $[h^{\cdot}]$ decreasing with increasing Mg concentration because the Mg donor dominates. However, models involving associates of Mg_{Al} with native defects such as

$$[Mg'_{Al}]=[(Mg_{Al}V_O)^{\cdot}]=\tfrac{1}{2}[Mg]_{total} \quad (20)$$

or

$$[Mg'_{Al}]=[(Mg_{Al}V_O)^{\cdot}]\,,$$

with

$$[(Mg_{Al}V_OMg_{Al})^x]=\tfrac{1}{2}[Mg]_{total} \quad (21)$$

or corresponding ones with $Al_i^{\cdots}$ instead of $V_O^{\cdot\cdot}$, lead to $[V_O^{\cdot\cdot}]$ and $[Al_i^{\cdots}]$ increasing with [Mg] and are acceptable. However, it is unlikely that pairs are dominant species at the relatively high temperatures of measurement and the low concentrations of Mg. Therefore, the further analysis will be based on the models with single defects with the electroneutrality conditions governed by either Eq. (9) or (11).

Anomalous oxygen-pressure dependence

As seen in Fig. 14, range I, $[Mg^x_{Al}]_{25\,°C}\approx[Mg^x_{Al}]_T$ should vary $\propto p_{O_2}^{1/4}$ when p_{O_2} is reduced. Yet according to Fig. 5 such a variation is observed at most over a narrow range of p_{O_2}, a sharp cutoff of $[Mg^x_{Al}]_{25\,°C}$ occurring at a critical oxygen pressure that is almost independent of the temperature of anneal. Such a cutoff can be explained if the sample contains centers other than Mg_{Al} with levels above the Mg'_{Al} level but close enough to ensure that the levels are occupied by electrons at high temperature. Holes trapped by Mg'_{Al} at high temperature (forming Mg^x_{Al}) tend to transfer to the higher levels upon cooling:

$$[Mg^x_{Al}]_{25\,°C}=[Mg^x_{Al}]_T-\Delta_T\,, \quad (22)$$

Δ_T being the concentration of occupied hole-trapping levels at high temperature. Possible candidates are Fe'_{Al}, Ni'_{Al}, and Co'_{Al} and deep donors. Ni and Co can be eliminated because they were not found in the analyses. Fe is present at a concentration of $\sim 4\times 10^{17}$ cm^{-3}, but the Fe'_{Al} level, lying >3 eV above the Mg'_{Al} level[35] is too high to contain enough electrons at high temperature to be able to absorb the $\sim 2\times 10^{17}$ cm^{-3} holes required to cause the cutoff: The Fe is present almost exclusively as Fe^x_{Al}. The same objection applies to shallow donors. A simple calculation shows that 4×10^{17} cm^{-3} deep donors with a level ≤ 1 eV above the Mg'_{Al} would have enough of its levels occupied by electrons to be able to account for the cutoff. Trivalent iron Fe^x_{Al} fulfills the concentration requirement and is believed to also fulfill the level position requirements. Figure 15 shows isotherms at high temperature and after cooling for model *A* in the presence of Fe.

According to Fig. 5, the boundary of ranges I and II at 1500 and 1600 °C is at $(p_{O_2})_{I,II}\approx 150$ Pa, but the conductivity results of Fig. 1 indicate a much smaller value of 10^{-3} Pa. For models *A* and *C*, $(p_{O_2})_{I,II}$ is proportional to $[Mg]^{-2}$ and $[Mg]^{-4/3}$, respectively. For the sample of Ref. 3, $(p_{O_2})_{I,II}\approx 10^{-2}$ atm $=10^3$ Pa at 1500 °C. In that sample the Mg content was believed to be 3.7×10^{17} cm^{-3}. However, that concentration leads to an ionic mobility that is ~ 6 times too small. Assuming this to be due to an underestimation of compensation, the concentration of active Mg in that sample must have been 6×10^{16} cm^{-3}. On this basis we expect the boundary at 1500 °C in our sample with 8×10^{17} cm^{-3} Mg to be at 28 Pa for the $V_O^{\cdot\cdot}$ model, at 92 Pa for the $Al_i^{\cdot\cdot\cdot}$ model, not too far from the value indicated by Fig. 5, but considerably larger than deduced from $\sigma_i=\sigma t_i$ in Fig. 1. We believe the higher values to be the more reliable, those of Fig. 1 being in error due to an error in the emf's and the t_i's deduced from them as suggested in Fig. 2.

Temperature dependence of mobility, oxidation, and solubility

Let us now return to the conductivity results. If $Al_i^{\cdot\cdot\cdot}$ is a dominant species, i.e., model *C* holds, the modified experimental data for σ_i in Fig. 1 at low p_{O_2} where $[Mg'_{Al}]=[Mg]_{total}=8\times 10^{17}$ cm^3 can be represented with an $Al_i^{\cdot\cdot\cdot}$ mobility, measured in m^2 V^{-1} s^{-1},

$$[\mu(Al_i^{\cdot\cdot\cdot})]_{\|c}=2.2\times 10^5\exp[(-4.84\text{ eV})/kT]\ . \tag{23}$$

The activation energy is close to a calculated value 4.65 eV.[36] With $[Al_i^{\cdot\cdot\cdot}]N=\frac{1}{3}[Mg]N=2.7\times 10^{17}$ cm^{-3} (where $N=2.34\times 10^{22}$ cm^{-3}, the concentration of Al_2O_3 molecules per cm^3), measured in Ω^{-1}m^{-1},

$$(\sigma_i)_{\text{low }p_{O_2}}=2.3\times 10^{10}\exp[(-4.84\text{ eV})/kT]\ . \tag{24}$$

Subtraction of σ_i according to this formula from σ of curve 5 in Fig. 3 gives curve 7 for σ_h at $p_{O_2}=10^{-4}$ Pa as represented by Eq. (3).

If $V_O^{\cdot\cdot}$ is the dominant native ionic species (model *A*), $[Al_i^{\cdot\cdot\cdot}]$ is related to that of $V_O^{\cdot\cdot}$ through the Schottky and Frenkel disorder processes [Table I, relations (j) and (k)]:

$$[Al_i^{\cdot\cdot\cdot}]=(K_{F,Al}/K_S^{1/2})[V_O^{\cdot\cdot}]^{3/2}\ , \tag{25}$$

and therefore

$$\sigma_i=2^{-3/2}3q[Mg]^{3/2}N\frac{K_{F,Al}}{K_S^{1/2}}\mu(Al_i^{\cdot\cdot\cdot})\ , \tag{26}$$

where q is the electronic charge. Expression (23), which is measured in m^2 V^{-1} s^{-1}, now must be replaced by

$$2^{-3/2}3(Mg)^{1/2}\frac{K_{F,Al}}{K_S^{1/2}}[\mu(Al_i^{\cdot\cdot\cdot})]_{\|c}=2.2\times 10^5\exp(-4.84\text{ eV}/kT)\ , \tag{27}$$

the numbers being valid for $[Mg]N=8\times 10^{17}$ cm^{-3}. The activation energy of σ_i, $H(\mu_{Al})+H_{F,Al}-\frac{1}{2}H_S$ remains close to that computed for $\mu(Al_i^{\cdot\cdot\cdot})$ if $H_{F,Al}\approx\frac{1}{2}H_S$ as calculated by Catlow *et al.*[34] Expressions (23) or (27) give absolute values close to those reported for Al_2O_3:Co in which $[Co'_{Al}]\approx(8-10)\times 10^{17}$ cm^{-3},[10] close to the Mg content of the present crystal, but the activation energies are slightly different.

Equation (1) gives the hole conductivity of the unsaturated crystal in air. Using Table I, relations (d) and (e), one finds for model *A* dominated by $2[V_O^{\cdot\cdot}]=[Mg'_{Al}]$ with $[Mg]_{total}=[Mg^x_{Al}]$ [Fig. 15(a), region II],

$$(\sigma_h)_{\text{unsat},V}=q\mu_h N(\tfrac{1}{2}K_a^{Mg}K_4[Mg]_{total})^{1/3}p_{O_2}^{1/6}\ . \tag{28}$$

Comparison of (1) with (28) with $p_{O_2}=2\times 10^4$ Pa leads to

$$[\mu_h(K_a^{Mg}K_4)^{1/3}]_V=1.3\times 10^{-2}\times\exp[(-1.6\text{ eV})/kT]\ , \tag{29}$$

measured in cm^2 V^{-1} s^{-1} Pa$^{1/6}$.

According to Table I, relation (d), the hole concentration at low p_{O_2} (range I of model *A*) is given by

$$[h^{\cdot}]=2^{-1/2}K_4^{1/2}[\mathrm{Mg}]^{1/2}p_{O_2}^{1/4}$$

and thus

$$\mu_h^2K_4=2\sigma_h^2/([\mathrm{Mg}]N^2q^2p_{O_2}^{1/2}) . \quad (30)$$

With σ_h at $p_{O_2}=10^{-4}$ Pa as given by Eq. (3) we find

$$\mu_h^2K_4=1.78\times10^{-2}\exp[(-3.32\ \mathrm{eV})/kT] \quad (31)$$

in units of $\mathrm{cm^4\,V^2\,s^{-2}\,Pa^{-1/2}}$.

Equation (16) with $T^{3/2}\approx3.4\times10^5\exp[(-0.23\ \mathrm{eV})/kT]\ \mathrm{K^{3/2}}$ (valid from 1400 to 1600 °C) gives

$$K_a^{\mathrm{Mg}}=4\times10^{14}N^{-1}T^{3/2}\exp[(-0.68\ \mathrm{eV})/kT]$$
$$\approx5.8\times10^{-3}\exp[(-0.91\ \mathrm{eV})/kT] . \quad (32)$$

A combination of Eqs. (29), (31), and (32) gives

$$K_4=39.6\exp[(-2.18\ \mathrm{eV})/kT] , \quad (33)$$

measured in $\mathrm{Pa^{-1/2}}$, and

$$\mu_h=2.1\times10^{-2}\exp[(-0.57\ \mathrm{eV})/kT] , \quad (34)$$

which is measured in $\mathrm{cm^2\,V^{-1}\,s^{-1}}$. The activation energy of (33) is to be compared with the value 1.44 eV calculated by Catlow *et al.*[34] The expression for μ_h fits a small-polaron model but not the band model on which the analysis was based. However, relatively small adjustments in the activation energy of σ_h can remove the discrepancy, reducing the activation energy of Eq. (34) to zero. The present values of the constants give for the oxygen pressure at the boundary between regions I and II, measured in Pa,

$$(p_{O_2})_{\mathrm{I,II}}=2^2(K_a^{\mathrm{Mg}})^4/K_4^2[\mathrm{Mg}]^2$$
$$=2.5\times10^{-3}\exp[(0.72\ \mathrm{eV})/kT] \quad (35)$$

weakly dependent on temperature, with $(p_{O_2})_{\mathrm{I,II}}=0.3$ Pa at 1500 °C, a value smaller than expected from Fig. 5.

In the temperature region below 1360 °C the crystal is saturated and in equilibrium with a second phase of $MgAl_2O_4$. Then $[\mathrm{Mg'_{Al}}]$ is a function of temperature through relation (g), Table I:

$$[V_O^{\cdot\cdot}]=\tfrac{1}{2}[\mathrm{Mg'_{Al}}]=2^{2/3}(K_{\mathrm{sol},V}^{\mathrm{Mg}})^{1/3}a_{\mathrm{MgO}}^{2/3} . \quad (36)$$

Use of relation (d) leads to

$$(\sigma_h)_{\mathrm{sat},V}=q\mu_hN[h^{\cdot}]$$
$$=2^{1/3}q\mu_hNK_4^{1/2}(K_{\mathrm{sol},V}^{\mathrm{Mg}})^{1/6}a_{\mathrm{MgO}}^{1/3}p_{O_2}^{1/4} . \quad (37)$$

This relation holds independent of whether the crystal is in range I or II. Comparison with Eq. (2) with $p_{O_2}=2\times10^4$ Pa gives

$$\mu_hK_4^{1/2}(K_{\mathrm{sol},V}^{\mathrm{Mg}})^{1/6}a_{\mathrm{MgO}}^{1/3}=2.39\times10^{-2}$$
$$\times\exp[(-2.4\ \mathrm{eV})/kT] , \quad (38)$$

measured in $\mathrm{cm^2\,V^{-1}\,s^{-1}\,Pa^{-1/4}}$, and combination of Eq. (38) with Eqs. (29) and (31) gives

$$K_{\mathrm{sol},V}^{\mathrm{Mg}}a_{\mathrm{MgO}}^2=3.3\times10^{-5}\exp[(-4.4\ \mathrm{eV})/kT] . \quad (39)$$

For Al_2O_3 with $a_{Al_2O_3}=1$ in equilibrium with precipitates of $MgAl_2O_4$,

$$a_{\mathrm{MgO}}=\exp(\Delta G/RT)\approx\exp(\Delta H/RT) , \quad (40)$$

ΔG and ΔH being the Gibbs free energy and enthalpy of reaction (i), Table I. By estimating $\Delta G\simeq\Delta H=-30$ kJ/mol $=-0.3$ eV, the combination of Eqs. (39) and (40) gives

$$K_{\mathrm{sol},V}^{\mathrm{Mg}}=3.3\times10^{-5}\exp[(-3.8\ \mathrm{eV})/kT] . \quad (41)$$

Analyzing in a similar manner the data on the basis of model *C* dominated by $[\mathrm{Mg'_{Al}}]\approx3[\mathrm{Al}_i^{\cdot\cdot\cdot}]$ leads to

$$K_3=7.1\times10^8\exp[(-3.48\ \mathrm{eV})/kT] , \quad (42)$$

$$\mu_h=1.2\times10^{-4}$$
$$\times\exp[(-0.5\ \mathrm{eV})/kT]\ \mathrm{cm^2\,V^{-1}\,s^{-1}} , \quad (43)$$

$$K_{\mathrm{sol},i}^{\mathrm{Mg}}=9.5\times10^5\exp[(-8.0\ \mathrm{eV})/kT] , \quad (44)$$

all giving acceptable values. Thus neither model *A* nor model *C* can be rejected. However, microscopic investigations by Pletka *et al.*[37] indicate that the $V_O^{\cdot\cdot}$ model is to be preferred. Therefore, results (32), (33), and (34) are probably the best, and further considerations will be based on the $V_O^{\cdot\cdot}$ model.

The solubility of magnesium is the sum of the solubilities of $\mathrm{Mg'_{Al}}$ and $\mathrm{Mg_{Al}^x}$. In the absence of compensating donors, the former is given by relation (g) of Table I with $a_{\mathrm{MgO}}^2K_{\mathrm{sol},V}^{\mathrm{Mg}}$ given by Eq. (39):

$$[\mathrm{Mg'_{Al}}]=2^{1/3}(K_{\mathrm{sol},V}^{\mathrm{Mg}}a_{\mathrm{MgO}}^2)^{1/3}$$
$$=4\times10^{-2}\exp[(-1.47\ \mathrm{eV})/kT] , \quad (45)$$

a result independent of the assumptions made regarding a_{MgO}. The contribution of $\mathrm{Mg_{Al}^x}$ is related to that of $\mathrm{Mg'_{Al}}$ through Table I, (b) with $K_{\mathrm{ox},V}^{\mathrm{Mg}}$ as given by (d). The contribution depends on oxygen pressure, measured in $\mathrm{Pa^{-1/4}}$,

TABLE III. Solubilities of Mg in parts per million by weight.[a]

	$N[Mg'_{Al}]$ Eq. (45)	$N[Mg^{x}_{Al}]$ Eq. (46)		$N[Mg]_{total}$ Eq. (46)				
T (°C)		$p_{O_2}=1$ Pa	$p_{O_2}=2\times10^4$ Pa	$p_{O_2}=1$ Pa	$p_{O_2}=10^4$ Pa	This paper (air)	Expt. Ref. 38 (vacuo)	Ref. 30 (wet H_2)
1360	0.27	0.06	0.7	0.3	0.94	8	8	
1600	1.0	0.55	6.5	2.55	8.5		100	
1630							130	150

[a]1 ppm Mg $\approx 10^{17}$ cm^{-3}.

$$[Mg^{x}_{Al}]=2^{-1/2}K_4^{1/2}(K_a^{Mg})^{-1}[Mg'_{Al}]^{3/2}p_{O_2}^{1/4}$$

$$=6.2\exp[(-2.39\text{ eV})/kT]p_{O_2}^{1/4}\ . \quad (46)$$

Table III gives the solubility of Mg calculated from Eqs. (45) and (46) at 1600 and 1360 °C under $p_{O_2}=1$ or 10^4 Pa and values *in vacuo* reported by Roy and Coble[38] (RC) which are represented by

$$[Mg]_{RC}=1.2\times10^4\exp[(-2.77\text{ eV})/kT]\ , \quad (47)$$

and by Peelen[30] in wet hydrogen.

The solubility at 1360 °C according to Eqs. (45) and (46) is $\simeq$8 times smaller than the 8 ppm it is according to our conductivity results which show that the sample becomes unsaturated at 1360 °C. On the other hand, the solubility expression of Roy and Coble, Eq. (47), gives almost exactly the experimental values. This expression also agrees closely with Peelen's 1630 °C value. Note that the values by Roy and Coble and Peelen were obtained at low-oxygen pressures, and thus should represent $[Mg]\approx[Mg'_{Al}]$ with a negligible contribution by Mg^{x}_{Al}. The discrepancy between the experimental values for the solubility and the theoretical values are probably due to errors in the activation energies. Similar errors may be responsible for the apparent activation energy of μ_h in Eqs. (34) and (43). In view of the uncertainty of the operation we shall not attempt to find the most probable place of these errors.

Discoloration-recoloration

Interaction with the atmosphere leading to a change in stoichiometry may or may not reach equilibrium in a reasonable time. The possibility of partial precipitation of MgO with formation of a spinel phase is another process that may or may not reach equilibrium. Under certain conditions the two may be related. This is actually the case for precipitation of MgO at high p_{O_2}. We have seen that the coloration of Al_2O_3:Mg is largely due to the formation of Mg^{x}_{Al} at high temperature as a result of oxidation according to relation (b), Table I, or, if precipitates of $MgAl_2O_4$ are present, relation (h) of Table I. Discoloration, therefore, may occur by two mechanisms—one involving, the other not involving, precipitation of $MgAl_2O_4$. In both cases oxygen has to be removed from the crystal, either by migration of oxygen out of the crystal or of aluminum into the crystal with evolution of O_2 at the surface. When charged defects are involved, this is an ambipolar process involving migration of ionic and electronic defects, the ones with the smaller concentration mobility product regulating the rate. In the present case this would be the ionic defects. If neutral defects are involved, only one species—the neutral one—is involved. In both cases discoloration proceeds by a front moving from the surface to the interior. At $T>1360$ °C no precipitation of MgO is involved. Further, diffusivities of Al and O are sufficiently large to cause discoloration upon reduction (and coloration upon oxidation) in a reasonably small time. At temperatures <1200 °C the diffusion coefficients of Al and O become so small that one does not expect coloration and discoloration to occur in a reasonable time and to be truly reversible, unless special effects come into play.

These effects probably involve precipitation: No discoloration occurred upon annealing at <950 °C of samples preannealed in air at $T>1650$ °C where it is presumed that nuclei of $MgAl_2O_4$ had been destroyed and where accordingly no precipitation of $MgAl_2O_4$ occurs at the lower temperature. If such nuclei are present, $MgAl_2O_4$ may precipitate according to Table I, relations (g) and (h), the latter causing discoloration with a front moving at a rate described by a diffusion constant as given by Eq. (6) with an activation energy of 0.8 eV. This activation energy is much smaller than that known for the normal self-diffusion of Al and O. Also, as seen in Fig. 6, the absolute value of the $\tilde{D}$ is much larger than that of D_{Al} or D_O. In comparing these diffusion coefficients it should be noted that the diffusion coefficient describing the front movement during discoloration is a chemical diffusion coefficient ($\tilde{D}_j$) which does not involve the concentration of the defect j whereas for self-diffusion $D_{self}=D_j[j]$. Since

$[j]\simeq 10^{-4}-10^{-6}$, this factor explains part of the difference between the D of the front and the self-diffusion coefficients of Al and O but not all of it, the observed ratio being much larger. So an additional effect must be involved.

Although the activation energy and the rate of the chemical D of the front are close to those observed at somewhat higher temperatures for chemical diffusion in Lucalox,[27] this correspondence is probably fortuitous: In Lucalox the effect was triggered by a change of p_{O_2} in the atmosphere, and the diffusion observed is believed to be grain boundary diffusion. In the present case, the effect is independent of p_{O_2} in the atmosphere and should be bulk diffusion. The observed independence from the oxidizing power of the atmosphere shows that the discoloration is not a simple reduction process. On the other hand, the conditions of the experiments rule out participation of hydrogen. Since the effect appears to be linked to the precipitation of $MgAl_2O_4$, this precipitation has to contain the clue. According to Table I, relation (h), precipitation should give rise to evolution of oxygen. If precipitation does not occur because oxygen is not removed, the urge to precipitate gives rise to an oxygen activity high enough to keep the Mg_{Al}^{x} in solution. Without inferring that a gas is actually present, this activity can be expressed as an oxygen pressure, $p_{O_2}^{*}$. This pressure can be calculated from the equilibrium constant of relation (h), Table I, which is equal to $(K_4 K_{sol,V}^{Mg})^{1/2}(K_a^{Mg})^{-1}$.

Owing to the cutoff resulting from the presence of iron, $p_{O_2}^{*}$ must be calculated as the pressure preventing $[Mg_{Al}^{x}]$ from being reduced to less than $\simeq\frac{1}{2}$ of its high-temperature value. In view of the fact that our expression for the solubility gives values that are $\simeq 8$ times too low we shall take a smaller value, $N[Mg_{Al}^{x}]/8=6\times 10^{16}$ cm^{-3}. Then, using Eq. (46) we find

$$p_{O_2}^{*}=1.42\times 10^{-26}\exp[(9.6\text{ eV})/kT]\text{ Pa}\ , \quad (48)$$

giving $(p_{O_2}^{*})_{900^\circ C}=2.6\times 10^{15}$ Pa$\approx 4.6\times 10^{10}$ atm and larger values at lower temperatures. Similarly, high values are found for the $Al_i^{\cdots}$ model.

Once the high oxygen activity is established, i.e., when some precipitation has occurred, diffusion will occur with the large activity difference inside and outside the crystal as the driving force. It is not surprising that with such a large pressure inside the crystal it is immaterial whether the pressure outside is 10^5 Pa or lower. The flux of oxygen out of the crystal is equal to $-D_j dc_j/dx$, D_j being the diffusion constant of the defect involved, and c its concentration, with $c_j=K_j' p_{O_2}^{*s}$, K_j being the equilibrium constant of the reaction forming the migrating defect. As a result, the activation energy of the chemical diffusion coefficient D from Eq. (6) will have contributions from both D_j and c_j, hence

$$H(\tilde{D})=0.8\text{ eV}=H(D_j)+H(c_j)\ , \quad (49)$$

or, since $H(c_j)=rH_j-9.78$ eV,

$$H(D_j)=0.8\text{ eV}-rH_j+9.6s\text{ eV}\ . \quad (50)$$

The values of r and s depend on the defect involved. This defect cannot be one of those dominant at normal p_{O_2}'s, $Al_i^{\cdots}$, or $V_O^{\cdot\cdot}$. For these $s<0$, and the high-oxygen pressure would reduce their concentration to practically zero, leading to slow in-diffusion of Al (as $Al_i^{\cdots}$) or out-diffusion of oxygen ($V_O^{\cdot\cdot}$ diffusing in) dependent on p_{O_2} in the ambient. Out-diffusion of O or in-diffusion of Al independent of the ambient are to be expected upon formation of interstitial oxygen or aluminum vacancies, formed at the extremely high-oxygen pressures indicated by Eq. (48). Values for r and s for various diffusion species and the corresponding values of $H(D_j)+rH_j$ are given in Table IV. Since a value of 3.8 eV has been reported for $H(D)$ of the last species[22] its formation energy H_j would have to be negative, which is impossible. Therefore, this species can be eliminated as a possibility. The most likely candidate at this stage is O_i^{x}. The same species has been found to be responsible for oxygen diffusion along grain boundaries[39] with energies corresponding to those of Table IV from 2.3 to 5.6 eV. It is conceivable that O_i^{x} is also responsible for oxygen bulk diffusion under normal conditions, for which activation energies of self-diffusion $[=H(D_j)+rH_j]$ of 6.59 ± 1.1 eV (Ref. 25), 7.68 eV (Ref. 40), 6.38 ± 0.4 (Ref. 41), and 6.7 eV (Ref. 42) have been observed.

It may be concluded that the conditions under which discoloration occurs at low temperatures are sufficiently special that the general conclusion that diffusion processes in acceptor-doped crystals are appreciably faster than those in donor-doped crystals[2] is not warranted. Effects similar to the ones discussed here have been found in the precipitation

TABLE IV. Values of r and s for different diffusing species, and the corresponding enthalpy values.

Species	r	s	$H(D_j)+rH_j$ (eV)
$O_{2,i}^{x}$	1	1	10.4
O_i^{x}	1	$\frac{1}{2}$	5.6
$O_i'+h^{\cdot}$	$\frac{1}{2}$	$\frac{1}{4}$	3.2
$O_i''+2h^{\cdot}$	$\frac{1}{3}$	$\frac{1}{6}$	2.4
$V_{Al}'''+3h^{\cdot}$	$\frac{1}{4}$	$\frac{3}{16}$	2.6

of excess oxygen in NiO,[43] and in the permeation of hydrogen through Al_2O_3.[44] In the latter, a large apparent permeation with a low activation energy found with decreasing temperature was attributed to evolution of "internally absorbed" hydrogen.

Although the explanation proposed above accounts for the discoloration at $T < 1000$ °C, it cannot explain the relatively rapid recoloration by annealing at $T > 900$ °C of samples discolored previously by annealing at $T < 900$ °C. The fact that the recoloration depends on the oxidizing power of the atmosphere indicates that the effect cannot be due to oxygen retained in the sample: in-diffusion of oxygen (or out-diffusion of aluminum) must be involved. Since the recoloration occurs without a front, oxygen must permeate quickly into the sample, leading to a homogeneous distribution of excess oxygen before coloration occurs. This can happen if oxygen penetrates along dislocations or subgrain boundaries, recoloration occurring when the oxygen diffuses into the surrounding material or the subgrains. Since only small distances are involved, the latter process may occur by normal bulk diffusion. Only the penetration along dislocations or subgrain boundaries has to be abnormally rapid. The slow increase of coloration after an initial rapid discoloration of a preoxidized sample seen in Fig. 9 curve *a* must be attributed to redistribution of holes between the Mg'_{Al} level and empty levels lying below it. The effects for samples prefired at low p_{O_2} (curves *c* and *d* of Fig. 9) may involve reoxidation of the sample close to the surface by oxygen diffusing in from the surface or by Al diffusing out with its normal diffusion constant.

There is considerable similarity between the systems MgO:Li and Al_2O_3:Mg; in both cases oxidation leads to neutral acceptor centers Li^x_{Mg},Mg^x_{Al} consisting of the effectively negative acceptors with an effectively positive O^- ($\equiv O_O^{\cdot}$) next to it, and showing an optical absorption band characteristic of the latter.[45] The Li^x_{Mg} centers in MgO also increase the hole conductivity[46,47] with an energy of liberation of the hole of 0.6—0.72 eV (Ref. 48) similar to that found for Mg^x_{Al} in this paper.

The hole-release energy of 0.68 eV, deduced from our studies of the rate of bleaching of photocreated Mg^x_{Al} centers at -20 °C, is close to a theoretical value of 0.56 ± 0.2 eV calculated for the thermal separation between the Mg'_{Al} level and the valence band using the small-polaron model for the free hole (O^- ion on an O^{2-} site).[34] A large-polaron model would give a computed value that is 0.4 eV smaller.[33] Yet the results presented in the present paper indicate that free holes behave as large polarons with $E_a = 0.68$ eV.

SUMMARY

High-temperature measurements of electronic and ionic conductivity of Al_2O_3:8 ppm Mg as $f(p_{O_2}, T)$ show the crystal to be unsaturated at $T > 1360$ °C, saturated below this temperature. Optical absorption and ESR studies show that, at high p_{O_2}, Mg is mainly present as neutral Mg^x_{Al}. Analysis of the results on the basis of a point-defect model leads to values of basic thermodynamic parameters. Discoloration of oxidized crystals at $T < 1000$ °C proceeds from the surface inwards with a front moving with an unexpectedly large rate which is attributed to the establishment of extremely high effective oxygen pressures as a result of precipitation of $MgAl_2O_4$. Subsequent coloration at $T < 1200$ °C proceeds without a front and may involve penetration of oxygen along dislocations or subgrain boundaries.

Low-temperature hole-release studies in photoexcited Al_2O_3:Mg + Fe and Mg + Cr show the Mg^x_{Al} hole-binding energy to be $\simeq 0.68$ eV. Holes probably move as large polarons.

ACKNOWLEDGMENT

This work was supported by the U.S. Department of Energy under Contract No. AS03-76 SF00113, Project Agreement AT03-76 ER71027.

[1] R. T. Cox, J. Phys. (Paris), Colloq. 34, C-9, 333 (1973).
[2] R. T. Cox, Solid State Commun. 9, 1989 (1971).
[3] S. K. Mohapatra and F. A. Kröger, J. Am. Ceram. Soc. 60, 141 (1977).
[4] F. A. Kröger and H. J. Vink, in *Solid State Physics*, edited by F. Seitz and D. Turnbull (Academic, New York, 1956), Vol. 3, p. 307.
[5] F. A. Kröger, *The Chemistry of Imperfect Crystals* (North-Holland, Amsterdam, 1974), Vol. 2, p. 14.
[6] S. K. Mohapatra and F. A. Kröger, J. Am. Ceram. Soc. 61, 106 (1978).
[7] K. Hauffe and D. Hoeffgen, Ber. Bunsenges. Phys. Chem. 74, 537 (1970).
[8] R. Mueller and H. H. Guenthard, J. Chem. Phys. 44, 365 (1966).
[9] S. K. Tiku and F. A. Kröger, J. Am. Ceram. Soc. 63, 31 (1980).
[10] B. V. Dutt, J. P. Hurrell, and F. A. Kröger, J. Am. Ceram. Soc. 58, 420 (1975).
[11] M. G. Townsend and O. F. Hill, Trans. Faraday Soc.

61, 2597 (1965).
[12]J. J. Rasmussen and W. D. Kingery, J. Am. Ceram. Soc. 53, 436 (1970).
[13]R. T. Cox, Ph.D. thesis, Université de Grenoble I, 1972 (unpublished).
[14]R. H. Hoskins and B. H. Soffer, Phys. Rev. 133, A490 (1964).
[15]T. P. Jones, R. H. Coble, and C. J. Mogab, J. Am. Ceram. Soc. 52, 331 (1969).
[16]Te-Tse Chang, D. Foster, and A. H. Kahn, J. Res. Natl. Bur. Stand. 83, 133 (1978).
[17]D. L. Dexter, in *Solid State Physics,* edited by F. Seitz and D. Turnbull (Academic, New York, 1958), Vol. 6, p. 353.
[18]Y. Chen and W. A. Sibley, Phys. Rev. 154, 842 (1967).
[19]F. A. Modine, Phys. Rev. B 16, 5528 (1977).
[20]N. Koumvakalis, J. Appl. Phys. 51, 5528 (1980).
[21]O. F. Schirmer, Z. Phys. B 24, 235 (1976).
[22]S. K. Mohapatra and F. A. Kröger, J. Am. Ceram. Soc. 60, 381 (1977).
[23]E. M. Okul'yonok, J. Solid State Chem. 26, 17 (1978).
[24]A. E. Paladino and W. D. Kingery, J. Chem. Phys. 37, 957 (1965).
[25]Y. Oishi and W. D. Kingery, J. Chem. Phys. 33, 480 (1960).
[26]D. J. Reed and B. J. Wuensch, Bull. Am. Ceram. Soc. 56, 298 (1977).
[27]K. Kitizawa and R. L. Coble, J. Am. Ceram. Soc. 57, 250 (1974).
[28]W. C. Johnson, J. Am. Ceram. Soc. 61, 234 (1978).
[29]A. Munitz, M. Metzger, and R. Mehrabian, Metall. Trans. AIME 10A, 1491 (1979).
[30]J. G. J. Peelen, Ph.D. thesis, Eindhoven University of Technology, 1977 (unpublished).
[31]M. A. Brown, J. Phys. C 10, 4939 (1977).
[32]R. A. Evarestov, A. N. Ermoskin, and V. A. Lovchikov, Phys. Status Solidi B 99, 387 (1980).
[33]E. A. Colbourn and W. C. Mackrodt, Solid State Commun. 40, 265 (1981).
[34]C. R. A. Catlow, R. James, W. C. Mackrodt, and R. F. Stewart, Phys. Rev. B 25, 1006 (1982).
[35]S. K. Tiku and F. A. Kröger, J. Am. Ceram. Soc. 63, 31 (1980).
[36]G. J. Dienes, D. O. Welch, C. R. Fischer, R. D. Hatcher, O. Lazareth, and M. Samberg, Phys. Rev. B 11, 3060 (1975).
[37]B. J. Pletka, T. E. Mitchell, and A. H. Heuer (unpublished) [work referred to in A. H. Heuer, J. Am. Ceram. Soc. 62, 317 (1979)].
[38]S. K. Roy and R. L. Coble, J. Am. Ceram. Soc. 51, 1 (1968).
[39]H. A. Wang and F. A. Kröger, J. Am. Ceram. Soc. 63, 613 (1980).
[40]D. J. Reed and B. J. Wuensch, J. Am. Ceram. Soc. 63, 88 (1980).
[41]K. P. R. Reddy, Ph.D. thesis, Case Western Reserve University, 1979 (unpublished).
[42]Y. Oishi, K. Ando, and Y. Kubota, J. Chem. Phys. 73, 1410 (1980).
[43]R. Farhi, G. Pétot-Ervas, and F. A. Kröger, Proceedings of the 9th International Symposium on the Reactivity of Solids, Cracow, 1980 (Elsevier, New York, in press).
[44]R. M. Roberts, T. S. Elleman, H. Palmour III, and K. Verghese, J. Am. Ceram. Soc. 62, 495 (1979).
[45]J. L. Boldu, M. M. Abraham, and Y. Chen, Phys. Rev. B 19, 4421 (1979).
[46]Y. Chen, M. M. Abraham, J. L. Boldu, and V. M. Orera, J. Phys. (Paris), Colloq. 41, C-6, 398 (1980).
[47]Y. Chen and R. H. Kernohan, Solid State Commun. 33, 441 (1980).
[48]D. J. Eisenberg, L. S. Cain, K. H. Lee, and J. H. Crawford, Jr., Appl. Phys. Lett. 33, 479 (1978).

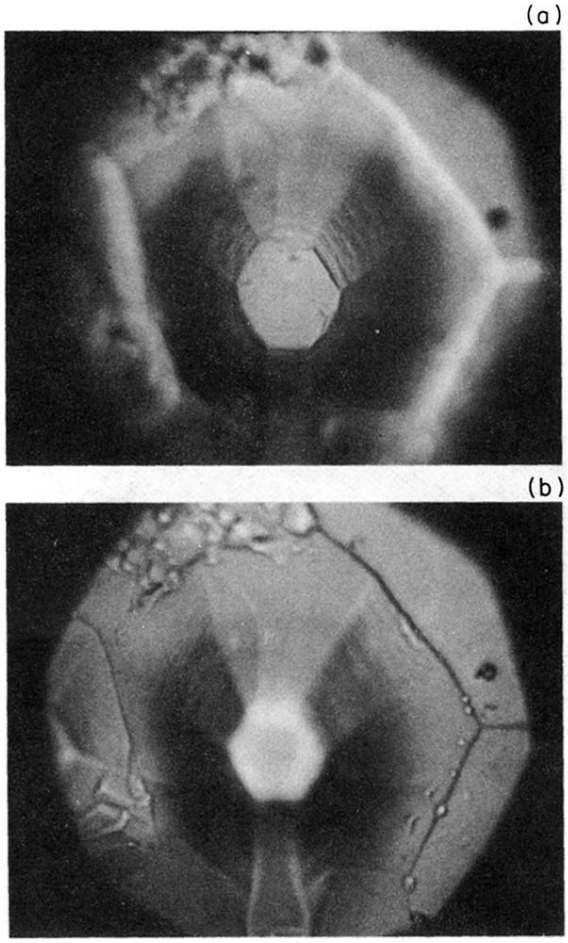

FIG. 10. Microscope picture (magnification 400×) of the surface of a crystal discolored by a prolonged anneal at 900 °C etched for 10 min with borax at 800 °C.

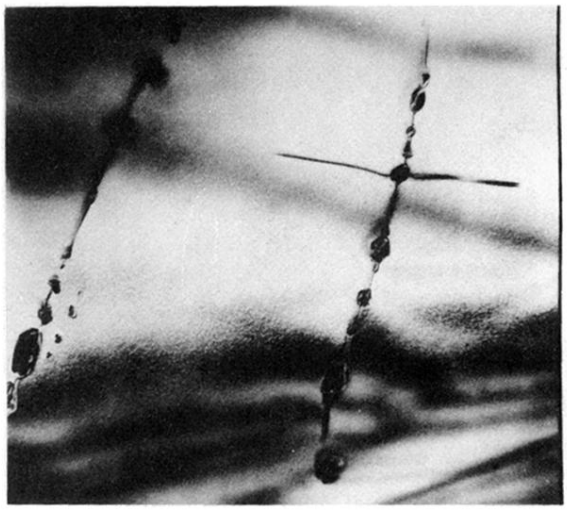

FIG. 11. TEM picture (magnification 8500×) showing the presence of precipitates along dislocation lines.

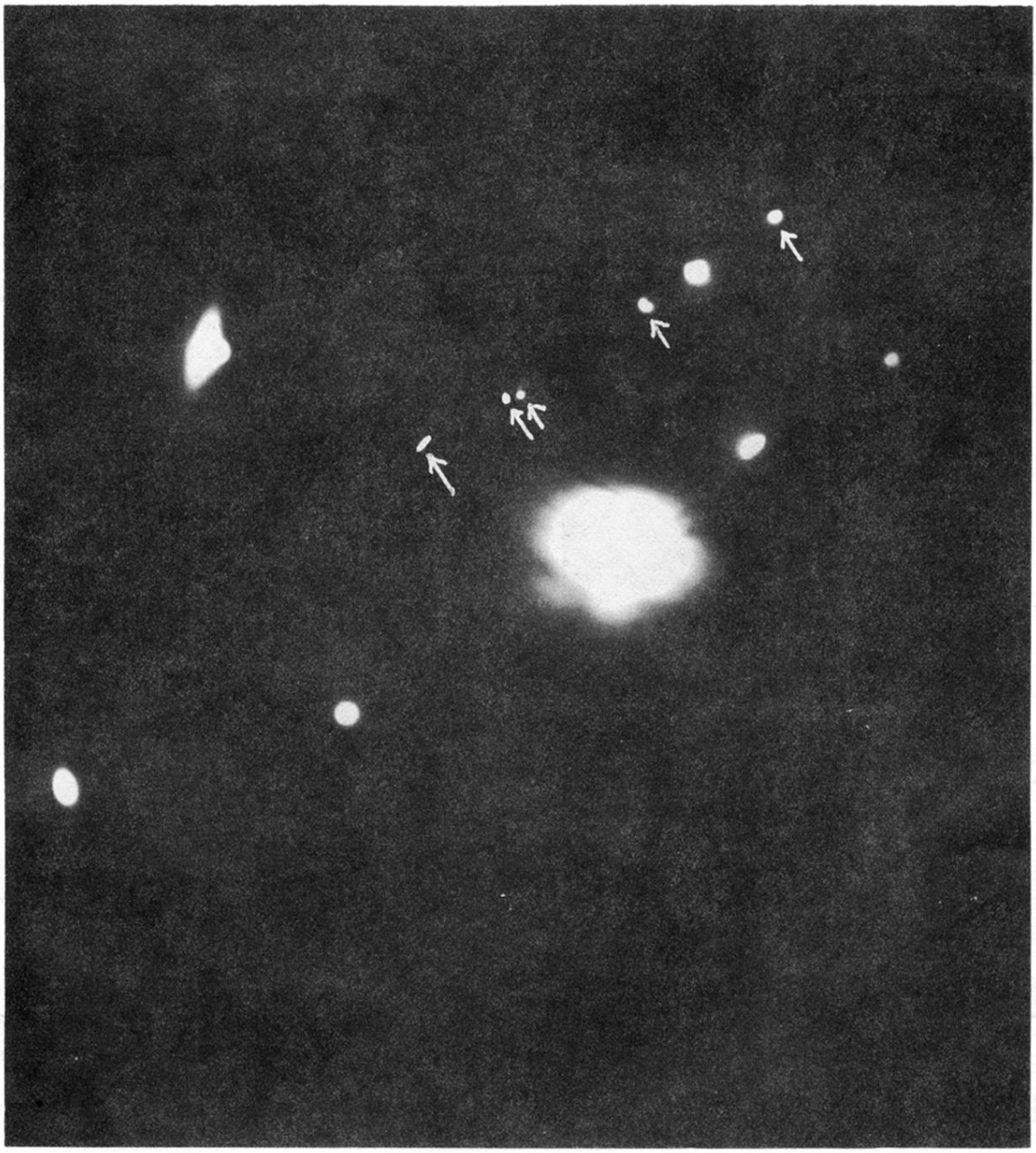

FIG. 12. Electron diffraction pattern of a precipitate and its surroundings show the spots due to Al_2O_3 and extra spots caused by the precipitate (the latter marked by arrows).